NASA Contractor Report 178206

ICASE REPORT NO. 86-69

ICASE

(NASA-CR-178206) ON THE NONLINEARITY OF MODERN SHOCK-CAPTURING SCHEMES Final Report (NASA) 63 p CSCL 51A

N87-13410

Unclas

G3/02 43954

ON THE NONLINEARITY OF MODERN SHOCK-CAPTURING SCHEMES

Ami Harten

Contract Nos. NAS1-17070, NAS1-18107

October 1986

INSTITUTE FOR COMPUTER APPLICATIONS IN SCIENCE AND ENGINEERING
NASA Langley Research Center, Hampton, Virginia 23665

Operated by the Universities Space Research Association

NASA

National Aeronautics and
Space Administration

Langley Research Center
Hampton, Virginia 23665

ON THE NONLINEARITY OF MODERN SHOCK-CAPTURING SCHEMES

Ami Harten
School of Mathematical Sciences, Tel-Aviv University
and
Department of Mathematics, UCLA

Dedicated to Peter Lax on his 60th birthday

Abstract

In this paper, we review the development of shock-capturing methods, paying special attention to the increasing nonlinearity in the design of numerical schemes. We study the nature of this nonlinearity and examine its relation to upwind differencing. This nonlinearity of the modern shock-capturing methods is essential, in the sense that linear analysis is not justified and may lead to wrong conclusions. Examples to demonstrate this point are given.

Research was supported in part by the National Aeronautics and Space Administration under NASA Contract Nos. NAS1-17070 and NAS1-18107 while the author was in residence at the Institute for Computer Applications in Science and Engineering (ICASE), NASA Langley Research Center, Hampton, VA 23665-5225.

1. INTRODUCTION

In this paper, we describe and analyze numerical techniques that are designed to approximate weak solutions of hyperbolic systems of conservation laws in several space dimensions. For sake of exposition, we shall describe these methods as they apply to the pure initial value problems (IVP) for a one-dimensional scalar conservation law

$$(1.1) \qquad u_t + f(u)_x = 0, \qquad u(x,0) = u_0(x).$$

To further simplify our presentation, we assume that the flux $f(u)$ is a convex function, i.e., $f''(u) > 0$ and that the initial data $u_0(x)$ are piecewise smooth functions which are either periodic or of compact support. Under these assumptions, no matter how smooth u_0 is, the solution $u(x,t)$ of the IVP (1.1) becomes discontinuous at some finite time $t = t_c$. In order to extend the solution for $t > t_c$, we introduce the notion of weak solutions, which satisfy

$$(1.2a) \qquad \frac{d}{dt}\int_a^b u\,dx + f(u(b,t)) - f(u(a,t)) = 0$$

for all $b \geq a$ and $t \geq 0$. Relation (1.2a) implies that $u(x,t)$ satisfies the PDE in (1.1) wherever it is smooth, and the Rankine-Hugoniot jump relation

$$(1.2b) \qquad f(u(y + 0,t)) - f(u(y - 0,t)) = [u(y + 0,t) - u(y - 0,t)]\,\frac{dy}{dt}$$

across curves $x = y(t)$ of discontinuity.

It is well known that weak solutions are not uniquely determined by their initial data. To overcome this difficulty, we consider the IVP (1.1) to be the vanishing viscosity limit $\varepsilon \downarrow 0$ of the parabolic problem

$$(1.3a) \qquad (u^\varepsilon)_t + f(u^\varepsilon)_x = \varepsilon(u^\varepsilon)_{xx}, \qquad u^\varepsilon(x,0) = u_0(x),$$

and identify the unique "physically relevant" weak solution of (1.1) by

$$(1.3b) \qquad u = \lim_{\varepsilon \downarrow 0} u^\varepsilon.$$

The limit solution (1.3) can be characterized by an inequality that the values $u_L = u(y - 0,t)$, $u_R = u(y + 0,t)$ and $s = dy/dt$ have to satisfy; this inequality is called an entropy condition; admissible discontinuities are called shocks. When $f(u)$ is convex, this inequality is equivalent to Lax's shock condition

$$(1.4) \qquad a(u_L) > s > a(u_R)$$

where $a(u) = f'(u)$ is the characteristic speed (see [20] for more details).

We turn now to describe finite difference approximations for the numerical solution of the IVP (1.1). Let v_j^n denote the numerical approximation to $u(x_j,t_n)$ where $x_j = jh$, $t_n = n\tau$; let $v_h(x,t)$ be a globally defined numerical approximation associated with the discrete values $\{v_j^n\}$, $\infty < j < \infty$, $n \geq 0$.

The classical approach to the design of numerical methods for partial differential equations is to obtain a solvable set of equations for $\{v_j^n\}$

by replacing derivatives in the PDE by appropriate discrete approximations. Therefore, there is a conceptual diffficulty in applying classical methods to compute solutions which may become discontinuous. Lax and Wendroff [21] overcame this difficulty by considering numerical approximations to the *weak formulation* (1.2a) rather than to the PDE (1.1). For this purpose, they have introduced the notion of schemes in conservation form:

$$\text{(1.5a)} \qquad v_j^{n+1} = v_j^n - \lambda(\bar{f}_{j+1/2} - \bar{f}_{j-1/2}) \equiv (E_h \cdot v^n)_j;$$

here $\lambda = \tau/h$ and $\bar{f}_{i+1/2}$ denotes

$$\text{(1.5b)} \qquad \bar{f}_{i+1/2} = f(v^n_{i-k+1}, \ldots, v^n_{i+k});$$

$\bar{f}(w_1,\ldots,w_{2k})$ is a numerical flux function which is consistent with the flux $f(u)$, in the sense that

$$\text{(1.5c)} \qquad \bar{f}(u,u,\ldots u) = f(u);$$

E_h denotes the numerical solution operator. Lax and Wendroff proved that if the numerical approximation converges boundedly almost everywhere to some function u, then u is a weak solution of (1.1), i.e., it satisfies the weak formulation (1.2a). Consequently discontinuities in the limit solution automatically satisfy the Rankine-Hugoniot relation (1.2b). We refer to this methodology as shock-capturing (a phrase coined by H. Lomax).

In the following, we list the numerical flux function of various 3-point schemes ($k = 1$ in (1.5b)):

(i) The Lax-Friedrichs scheme [19]

$$\bar{f}(w_1,w_2) = \frac{1}{2}\left[f(w_1) + f(w_2) - \frac{1}{2}(w_2 - w_1)\right] \tag{1.6}$$

(ii) Godunov's scheme [5]

$$\bar{f}(w_1,w_2) = f(V(0;w_1,w_2)); \tag{1.7a}$$

here $V(x/t;\ w_1,w_2)$ denotes the self-similar solution of the IVP (1.1) with the initial data

$$u_0(x) = \begin{cases} w_1 & x < 0 \\ w_2 & x > 0 \end{cases}. \tag{1.7b}$$

(iii) The Cole-Murman scheme [26]:

$$\bar{f}(w_1,w_2) = \frac{1}{2}\left[f(w_1) + f(w_2) - |\bar{a}(w_1,w_2)|(w_2 - w_1)\right] \tag{1.8a}$$

where

$$\bar{a}(w_1,w_2) = \begin{cases} \dfrac{f(w_2) - f(w_1)}{w_2 - w_1} & \text{if} \quad w_1 \neq w_2 \\ a(w_1) & \text{if} \quad w_1 = w_2 \end{cases}. \tag{1.8b}$$

(iv) The Lax-Wendroff scheme [21]:

$$\bar{f}(w_1,w_2) = \frac{1}{2}\left\{f(w_1) + f(w_2) - \lambda a\left(\frac{w_1 + w_2}{2}\right)[f(w_2) - f(w_1)]\right\}. \tag{1.9}$$

(v) MacCormack's scheme [24]:

$$\bar{f}(w_1,w_2) = \frac{1}{2}\{f(w_2) + f(w_1 - \lambda[f(w_2) - f(w_1)])\}. \tag{1.10}$$

Let $E(t)$ denote the evolution operator of the exact solution of (1.1) and let E_h denote the numerical solution operator defined by the RHS of (1.5a). We say that the numerical scheme is r-th order accurate (in a pointwise sense) if its local truncation error satisfies

$$E(\tau) \cdot u - E_h \cdot u = O(h^{r+1}) \tag{1.11}$$

for all sufficiently smooth u; here $\tau = O(h)$. If $r > 0$, we say that the scheme is consistent.

The schemes of Lax-Friedrichs (1.6), Godunov (1.7) and Cole-Murman (1.8) are first order accurate; the schemes of Lax-Wendroff (1.9) and MacCormack are second order accurate.

We remark that the Lax-Wendroff theorem states that if the scheme is convergent, then the the limit solution satisfies the weak formulation (1.2b); however, it need not be the entropy solution of the problem (see [11]). It is easy to see that the schemes of Cole-Murman (1.8), Lax-Wendroff (1.9) and MacCormack (1.10) admit a stationary "expansion shock" (i.e., $f(u_L) = f(u_R)$ with $a(u_L) < a(u_R)$) as a steady solution. This problem can be easily rectified by adding sufficient numerical dissipation to the scheme (see [25] and [10]).

The cardinal problem that is yet to be resolved is the question of convergence of the numerical approximation.

2. LINEAR STABILITY AND COMPUTATION OF WEAK SOLUTIONS

Let us consider the constant coefficient case $f(u) = au$, $a = \text{const.}$ in (1.1), i.e.,

$$u_t + au_x = 0, \qquad u(x,0) = u_0(x), \tag{2.1a}$$

the solution to which is

$$u(x,t) = u_0(x - at). \tag{2.1b}$$

In this case, all the schemes mentioned in the previous section, (1.6) - (1.10), take the form

$$v_j^{n+1} = \sum_{\ell=-k}^{k} C_\ell v_{j-\ell}^n \equiv (E_h \cdot v^n)_j, \tag{2.2}$$

where C_ℓ are constants independent of j (C_ℓ are polynomial functions of the CFL number $\nu = \lambda a$). We note that in the constant coefficient case Godunov's scheme is identical to that of Cole-Murman; the MacCormack scheme is identical to that of Lax-Wendroff. Since the numerical solution operator E_h of these schemes in the constant coefficient case becomes a linear operator, we shall refer to these schemes as essentially linear or just "linear" schemes.

Next we briefly review the convergence theory of linear schemes; we refer the reader to [29] for a detailed analysis.

We say that the numerical scheme is stable if

$$(2.3a)\qquad \|(E_h)^n\| \leq C \quad \text{for} \quad 0 \leq n\tau \leq T, \quad \tau = O(h).$$

The constant coefficient scheme (2.2) is stable if and only if it satisfies von Neumann's condition:

$$(2.3b)\qquad \left|\sum_{\ell=-k}^{k} C_\ell \, e^{-i\ell\xi}\right| \leq 1 \quad \text{for all} \quad 0 \leq \xi \leq \pi.$$

It is easy to verify that all the 3-point schemes (1.6) - (1.10) satisfy condition (2.3b) under the Courant-Friedrichs-Lewy (CFL) restriction

$$(2.4)\qquad |\nu| = |\lambda a| \leq 1,$$

and thus are linearly stable. The notion of stability (2.3a) is related to convergence through Lax's equivalence theorem, which states that a consistent linear scheme is convergent if and only if it is stable.

The accumulation of error in a computation with a linearly stable scheme (2.2) is linear, in the sense that if the local truncation error (1.11) is $O(h^{r+1})$, then after performing $N = T/\tau = O(h^{-1})$ time-steps, the error is $O(h^r)$, i.e.,

$$(2.5)\qquad u(x_j, N\tau) - v_j^N = O(h^r).$$

An immense body of work has been done to find out whether stability of the constant coefficient scheme with respect to all "frozen coefficients" associated with the problem, implies convergence in the variable coefficient case and in the nonlinear case.

In the variable coefficient case, where the numerical solution operator is linear and Lax's equivalence theorem holds, it comes out that the stability of the variable coefficient scheme depends strongly on the dissipativity of the constant coefficient one, i.e., on the particular way it damps the high-frequency components in the Fourier representation of the numerical solution.

In the nonlinear case, under assumptions of sufficient smoothness of the PDE, its solution and the functional definition of the numerical scheme, Strang proved that linear stability of the first variation of the scheme implies its convergence; we refer the reader to [29] for more details.

Although there is no rigorous theory to support the supposition that linearly stable schemes should converge in the case of discontinuous solutions of nonlinear problems, we find in practice that this is true in many (although not all) instances; when such a scheme fails to converge, we refer to this case as "nonlinear instability". The occurrence of a nonlinear instability is usually associated with insufficient numerical dissipation which triggers exponential growth of the high-frequency components of the numerical solution.

Next we present two shock-tube calculations by the scheme (1.5) with the numerical flux

$$\bar{f}(w_1,w_2) = \frac{1}{2}\{f(w_2) + f(w_1 - \lambda[f(w_2) - f(w_1)]) - \frac{\theta}{4}(w_2 - w_1)\}. \tag{2.6}$$

The shock-tube problem is modelled by a Riemann IVP for the one-dimensional Euler equations of compressible gas:

$$u_t + f(u)_x = 0, \quad u(x,0) = \begin{cases} u_L & x < 0 \\ u_R & x > 0 \end{cases} \tag{2.7a}$$

where

(2.7b) $$u = (\rho, q\rho, E)^T, \qquad f(u) = qu + (0, p, qp)^T$$

with

(2.7c) $$P = (\gamma - 1)(E - \frac{1}{2}\rho q^2).$$

Here ρ, q, p, and E are the density, velocity, pressure, and total energy, respectively. In these calculations, $\gamma = 1.4$ and

(2.7d) $$u_L = (0.445, 0.3111, 8.928), \quad u_R = (0.5, 0., 1.4275).$$

The exact solution to this Riemann problem consists of a shock propagating to the right followed by a contact discontinuity and a left-propagating rarefaction wave; it is shown by a continuous line in Figures 1 and 2. The numerical solution of (2.6) is shown in Figures 1 and 2 by circles.

Figure 1 shows the results of the second-order accurate MacCormack scheme, i.e., $\theta = 0$ in (2.6). Observe the large spurious oscillations at the shock and at the contact discontinuity -- this is a Gibbs-like phenomenon. Note that although the rarefaction wave is computed rather accurately, there are some spurious oscillations at its right endpoint due to the discontinuity in the first derivative there.

Figure 2 shows the results of the first-order accurate scheme (2.6) with $\theta = 1$. Observe that now the numerical solution is oscillation-free.

However, both the shock and the contact discontinuity are now smeared much more than the corresponding ones in Figure 1. Note the excessive rounding of the corners at the endpoints of the rarefaction wave.

It is important to understand that the Gibbs-phenomenon by itself is not an instability; this is self-evident when we consider the constant coefficient problem (2.1) with discontinuous initial data u_0. However, in compressible gas calculations, where both density and pressure are restricted to have nonnegative values, the Gibbs phenomenon may cause the numerical solution to get out of the physical domain. Attempting to replace negative values of density and pressure by positive ones makes the scheme nonconservative and may result in an exponential growth of the solution.

The comparison between Figure 1 $(\theta = 0)$ and Figure 2 $(\theta = 1)$ shows that the Gibbs phenomenon in the second-order accurate scheme can be controlled by the addition of a numerical viscosity term. To do so without losing the second-order accuracy, Lax and Wendroff [21] suggested to take in (2.6) $\theta = \theta(w_1,w_2)$ of the form

$$\theta(w_1,w_2) = \chi|a(w_2) - a(w_1)|; \tag{2.8}$$

here $a = f'(u)$ and χ is a dimensionless constant; observe that $\theta \equiv 0$ in the constant coefficient case.

Numerical experiments showed that as χ increases the size of the spurious oscillations decreases, but at the cost of increased smearing of the discontinuity. Furthermore, when χ is fixed, the size of the spurious oscillations increases with the strength of the shock. These observations indicate that the numerical viscosity term (2.8) does not have an approriate functional dependence on the parameters that control the Gibbs phenomenon. Consequently, the choice of a suitable value of χ is problem dependent, and the practical use of the numerical scheme requires several preliminary runs to "tune parameters".

Ideally, we would like to have high-order accurate schemes that are capable of propagating a shock wave without having any spurious oscillations. In the scalar case, this can be accomplished by designing schemes to be monotonicity preserving, i.e., to satisfy

$$\text{(2.9)} \qquad v \text{ monotone} \Longrightarrow E_h \cdot v \text{ monotone}.$$

Godunov [5] has considered this avenue of design in the constant coefficient case (2.1) and showed that monotonicity preserving *linear* schemes (2.2) are necessarily only first order accurate. For some time this result has been perceived as saying that high-order schemes are necessarily oscillatory. Only much later was it realized that Godunov's result applies only to linear schemes and that it is possible to design *nonlinear* high order accurate schemes that are monotonicity preserving (see [1], [22], [6], [23], [7], [2], and [30]). Schemes of this type are the "modern shock-capturing schemes" referred to in the title of this paper.

In the rest of this paper we concentrate on the design and analysis of such highly nonlinear schemes. Even in the constant coefficient case these schemes are nonlinear to the extent that does not justify the use of local linear stability. Therefore, we shall start our journey into the nonlinear world by introducing the notion of total variation stability, which is more suitable to handle this type of schemes.

3. TOTAL VARIATION STABILITY AND TVD SCHEMES

Glimm [4] has considered the numerical solution by a random choice method of an IVP for a system of conservation laws with initial data of small total variation, and proved existence of weak solutions by showing convergence of subsequences. Following ideas used in Glimm's convergence proof, we can formulate the following theorem for convergence to weak solutions.

Theorem 3.1: Let v_h be a numerical solution of a conservative scheme (1.5).

(i) If

$$TV(v_h(\cdot,t)) \leq C \cdot TV(u_0) \tag{3.1}$$

where $TV(\ )$ denotes the total variation in x and C is a constant independent of h for $0 \leq t \leq T$, then any refinement sequence $h \to 0$ with $\tau = O(h)$ has a convergent subsequence $h_j \to 0$ that converges in L_1^{loc} to a weak solution of (1.1).

(ii) If v_h is consistent with an entropy inequality which implies uniqueness of the IVP (1.1), then the scheme is convergent (i.e., all subsequences have the same limit, which is the unique entropy solution of the IVP (1.1)).

We remark that unlike convergence theorems of classical numerical analysis, in which one shows that the distance between the solution and its numerical approximation vanishes as $h \to 0$, the convergence argument in the above theorem relies on a combination of compactness and uniqueness; its relation to an existence proof is quite obvious (see [8] for more details).

Next we demonstrate the use of Theorem 3.1 to prove convergence of schemes in conservation form (1.5) which are monotone, i.e., are of the form

$$v_j^{n+1} = H(v_{j-k}^n, \ldots, v_{j+k}^n) = (E_h \cdot v^n)_j, \tag{3.2}$$

where H is a monotone nondecreasing function of each of its arguments in the interval $[a,b]$, $a = \min v_j^0$, $b = \max v_j^0$. We note that the schemes of Godunov (1.7), Lax-Friedrichs (1.6) and the first order scheme (2.6) with $\theta \equiv 1$, are all monotone.

We start by observing that the operator E_h in (3.2) is order preserving

$$u \geq v \implies E_h \cdot u \geq E_h \cdot v. \tag{3.3a}$$

Since E_h is also conservative,

$$\sum_j (E_h \cdot v)_j = \sum_j v_j \tag{3.3b}$$

it follows then from a Lemma of Crandall and Tartar (see [3]) that E_h is ℓ_1-contractive, i.e., for all u and v in ℓ_1

$$\|E_h \cdot u - E_h \cdot v\|_{\ell_1} \leq \|u - v\|_{\ell_1} \tag{3.3c}$$

(here $\|u\|_{\ell_1} = h \sum_j |u_j|$). Taking u to be a translate of v, i.e.,

$$u_j = v_{j+1} \quad \text{for all } j$$

we get from (3.3c) that

$$\text{(3.4a)} \qquad TV(E_h \cdot v) \leq TV(v)$$

where

$$\text{(3.4b)} \qquad TV(w) \equiv \sum_j |w_{j+1} - w_j|.$$

It follows then that the numerical solution satisfies (3.1) with $C = 1$; thus we have established the convergence of subsequences. To show that all limit solutions are the same, we can use an argument of Barbara Keyfitz in the appendix to [11], which shows that (3.3c) implies that the scheme is consistent with Oleinik's entropy condition. This shows that monotone schemes satisfy the requirements of Theorem 3.1 and thus are convergent.

Unfortunately, monotone schemes are necessarily only first order accurate (see [11]). However, once we give up the requirement (3.3a) that E_h be an order preserving operator and consider the larger class of schemes that satisfy only (3.4), i.e., schemes that are total-variation-diminishing (TVD), it becomes possible to obtain second order accuracy. Observe that TVD schemes are necessarily monotonicity preserving (see [7]).

The following theorem provides an almost complete characterization of TVD schemes (see [7], [8], and [18]).

Theorem 3.2: Let E_h be a numerical solution operator of the form

(3.5a) $$v_j^{n+1} = v_j^n + \sum_{\ell=-k}^{k-1} C_\ell(j)\, \Delta_{j-\ell-1/2} v^n \equiv (E_h \cdot v^n)_j,$$

where

(3.5b) $$\Delta_{i+1/2} v^n = v_{i+1}^n - v_i^n,$$

and $C_\ell(j)$ denotes some functional of v^n evaluated at j. Then E_h is TVD if (and only if)[1] the following relations hold:

(3.6a) $$C_{-1}(j-1) \geq C_{-2}(j-2) \ldots \geq C_{-k}(j-k) \geq 0$$

(3.6b) $$-C_0(j) \geq -C_1(j+1) \geq \ldots \geq -C_{k-1}(j+k-1) \geq 0$$

(3.6c) $$-C_0(j) + C_{-1}(j-1) \leq 1.$$

We turn now to consider the important case of $k = 1$ in (3.5), i.e.,

(3.7) $$v_j^{n+1} = v_j^n + C_{-1}(j)\Delta_{j+1/2} v^n + C_0(j)\Delta_{j-1/2} v^n;$$

we refer to (3.7) as an essentially 3-point scheme, because the coefficients $C_0(j)$ and $C_{-1}(j)$ may depend on more than just $\{v_{j-1}^n, v_j^n, v_{j+1}^n\}$. To see

---

[1] Theorem 3.2 is not a complete characterization of TVD schemes, since the representation of a given nonlinear scheme in the form (3.5) is not unique.

the relation between the form (3.7) and the conservation form (1.5) let us consider the scheme

(3.8a) $$v_j^{n+1} = v_j^n - \lambda(\bar{f}_{j+1/2} - \bar{f}_{j-1/2})$$

with

(3.8b) $$\bar{f}_{i+1/2} = \frac{1}{2}(f_i + f_{i+1} - q_{i+1/2}\Delta_{i+1/2}v^n).$$

It is easy to see that (3.8) can be rewritten in the form (3.7) with

(3.9a) $$C_{-1}(j) = \frac{\lambda}{2}(\bar{a}_{j+1/2} + q_{j+1/2})$$

(3.9b) $$C_0(j) = \frac{\lambda}{2}(\bar{a}_{j-1/2} - q_{j-1/2});$$

here $\bar{a}_{i+1/2} = \bar{a}(v_i^n, v_{i+1}^n)$, which is defined by (1.8b).

Applying Theorem 3.2 to the scheme (3.8), we get that it is TVD if

(3.10a) $$\lambda|\bar{a}_{j+1/2}| \leq \lambda q_{j+1/2} \leq 1.$$

We turn now to outline the modified flux approach for the construction of second order accurate TVD schemes (see [7]). To simplify our presentation we choose in (3.10a)

(3.10b) $$q_{j+1/2} = |\bar{a}_{j+1/2}|;$$

this makes (3.8) identical to the Cole-Murman scheme (1.8). We observe that the TVD property of this scheme does not depend on the particular value of f(u), but only on the CFL-like condition

$$\text{(3.10c)} \qquad \lambda|\bar{a}_{j+1/2}| \leq 1;$$

note that this condition involves only the *grid values* f_j. Consequently, if we apply this scheme to a modified flux $f_j^{mod} = f_j + g_j$, i.e.,

$$\text{(3.11a)} \qquad v_j^{n+1} = v_j^n - \lambda(\bar{f}_{j+1/2} - \bar{f}_{j-1/2})$$

$$\text{(3.11b)} \qquad \bar{f}_{j+1/2} = \frac{1}{2}\,[f_j + g_j + f_{j+1} + g_{j+1} - |\bar{a}_{j+1/2} + \bar{\gamma}_{j+1/2}|\Delta_{j+1/2}v^n]$$

where

$$\text{(3.11c)} \qquad \bar{\gamma}_{j+1/2} = (g_{j+1} - g_j)/\Delta_{j+1/2}v^n,$$

we can conclude that this scheme is TVD provided that

$$\text{(3.12)} \qquad \lambda|\bar{a}_{j+1/2} + \bar{\gamma}_{j+1/2}| \leq 1.$$

It is easy to verify by truncation error analysis that if

$$\text{(3.13a)} \qquad g_j = h\sigma(a)u_x + O(h^2)$$

where

$$\sigma(x) = \frac{1}{2}\,|x|\,(1 - \lambda|x|), \tag{3.13b}$$

then

$$\bar{f}_{j+1/2} = \bar{f}^{LW}_{j+1/2} + O(h^2), \tag{3.13c}$$

where $\bar{f}^{LW}$ is the numerical flux (1.9) of the second-order accurate Lax-Wendroff scheme.

In [7] we have taken g_j to be

$$g_j = m(\sigma(\bar{a}_{j-1/2})\Delta_{j-1/2}v^n,\quad \sigma(\bar{a}_{j+1/2})\Delta_{j+1/2}v^n) \tag{3.14a}$$

where

$$m(x,y) = \begin{cases} s \cdot \min(|x|,|y|) & \text{if } \operatorname{sgn}(x) = \operatorname{sgn}(y) = s \\ 0 & \text{otherwise} \end{cases}. \tag{3.14b}$$

Clearly g_j (3.14a) satisfies (3.13a) and consequently the resulting scheme is second-order accurate, except at local extrema where the $O(h^2)$ term in (3.13a) and (3.13c) fails to be Lipschitz continuous.

Next we show that due to this particular definition of g_j, the modified flux scheme (3.11) which is second-order accurate, is also TVD under the original CFL restriction (3.10c); this follows immediately from the following lemma.

Lemma 3.3.

(3.15a) (i) $$|\bar{\gamma}_{j+1/2}| \leq 2|\sigma(\bar{a}_{j+1/2})|$$

(3.15b) (ii) $\lambda\ |\bar{a}_{j+1/2}| < 1 \Longrightarrow \lambda\ |\bar{a}_{j+1/2} + \gamma_{j+1/2}| < 1.$

Proof: We note that m(x,y) (3.14b) satisfies $|m(x,y)| < \min\ (|x|, |y|)$.

Consequently

$$|g_{j+1}-g_j| < |g_j| + |g_{j+1}| < \min\ (|\sigma_{j-1/2}\Delta_{j-1/2}v^n|, |\sigma_{j+1/2}\Delta_{j+1/2}v^n|)$$

$$+ \min\ (|\sigma_{j+1/2}\Delta_{j+1/2}v^n|\ ,\ |\sigma_{j+3/2}\Delta_{j+3/2}v^n|)$$

$$< 2\ |\sigma(\bar{a}_{j+1/2})|\ |\Delta_{j+1/2}v^n|\quad ,$$

which proves (3.15a).

It follows therefore from (3.13b) and (3.15a) that

$$\lambda\ |\bar{a} + \gamma| < \lambda\ |\bar{a}| + \lambda|\bar{\gamma}| < \lambda|\bar{a}| + 2\lambda\ |\sigma(\bar{a})|$$

$$= \lambda|\bar{a}| + \lambda|\bar{a}|\ (1 - \lambda|\bar{a}|) < \lambda|\bar{a}| + 1 - \lambda|\bar{a}| = 1,$$

which proves this lemma.

We remark that the modified flux scheme (3.11), as the Cole-Murman scheme it is derived from, admits a stationary "expansion shock" as a steady solution. Replacing $q_{j+1/2} = |\bar{a}_{j+1/2}|$ in (3.10b) by

(3.16) $$q_{j+1/2} = \max(|\bar{a}_{j+1/2}|,\ \varepsilon/\lambda), \qquad \varepsilon > 0$$

results in a modified flux scheme which is entropy consistent (see [28]) and thus can be shown to be convergent by Theorem 3.1.

The choice (3.14) of g_j is by no means unique. It is easy to check that changing g_j to be

$$(3.14a)' \qquad g_j = \bar{m}\,(\sigma(\bar{a}_{j-1/2})\Delta_{j-1/2}v^n,\ \sigma(\bar{a}_{j+1/2})\,\Delta_{j+1/2}v^n)$$

with

$$(3.14b)' \qquad \bar{m}\,(x,y) = \begin{cases} x & \text{if } |x| < |y| \\ y & \text{if } |x| > |y| \end{cases}$$

or

$$(3.14a)'' \quad g_j = m(\,(1-\lambda|\bar{a}_{j-1/2}|)\,\Delta_{j-1/2}v^n,\ 1/2\,\sigma(a_j)\,(v_{j+1}^n - v_{j-1}^n)\,,$$
$$(1 - \lambda\ |\bar{a}_{j+1/2}|)\,\Delta_{j+1/2}v^n)$$

with

$$(3.14b)'' \qquad m(x,y,z) = m(m(x,y),z) \quad ,$$

does not alter the relations (3.13a) and (3.15a) which makes the modified flux scheme (3.11) a second-order accurate TVD scheme, under the original CFL restriction (3.10c).

The modified flux approach is not the only methodology to construct second order accurate TVD schemes (there are many ways to skin a nonlinear cat). In the next section, we shall describe the MUSCL scheme of van Leer [23]; other techniques are described in [30], [27], and [31]. Unfortunately, all TVD schemes, independent of their derivation, are only first order accurate at local extrema of the solution. Consequently, TVD schemes can be second-order accurate in the L_1 sense, but only first order accurate in the maximum norm (see [14] for more details).

4. GODONOV-TYPE SCHEMES

In this section we describe Godunov-type schemes which are an abstraction of Godunov's scheme (1.7) (see [5]) due to ideas in [23], [12], and [13].

We start with some notations: Let $\{I_j\}$ be a partition of the real line; let A(I) denote the interval-averaging (or "cell-averaging") operator

$$(4.1) \qquad A(I) \cdot w = \frac{1}{|I|} \int_I w(y)dy \ ;$$

let $\bar{w}_j = A(I_j) \cdot w$ and denote $\bar{w} = \{\bar{w}_j\}$. We denote the approximate reconstruction of w(x) from its given cell-averages $\{\bar{w}_j\}$ by $R(x;\bar{w})$. To be precise, $R(x;\bar{w})$ is a piecewise-polynomial function of degree (r-1), which satisfies

$$(4.2a) \qquad (\text{i}) \quad R(x;\bar{w}) = w(x) + O(h^r) \qquad \text{wherever } w \text{ is smooth}$$

$$(4.2b) \qquad (\text{ii}) \quad A(I_j) \cdot R(\cdot\,;\bar{w}) = \bar{w}_j \quad (\text{conservation}).$$

Finally, we define Godunov-type schemes by

$$(4.3a) \qquad v_j^{n+1} = A(I_j^{n+1}) \cdot E(\tau) \cdot R(\cdot\,;v^n) \equiv (\bar{E}_h \cdot v^n)_j$$

$$(4.3b) \qquad v_j^o = A(I_j^o)\, u_o \ ;$$

here $\{I_j^n\}$ is the partition of the real line at time t_n, and E(t) is the evolution operator of (1.1).

In the scalar case, both the cell-averaging operator $A(I_j)$ and the solution operator $E(\tau)$ are order-preserving, and consequently also total-variation diminishing (TVD); hence

$$(4.4) \qquad TV\,(\bar{E}_h \cdot \bar{w}) \leq TV\,(R\,(\cdot\,;\,\bar{w})).$$

This shows that the total variation of the numerical solution of Godunov-type schemes is dominated by that of the reconstruction step.

The original first-order accurate scheme of Godunov is (4.3) with the piecewise-constant reconstruction

$$(4.5) \qquad R\,(x\,;\,\bar{w}) = \bar{w}_j \quad , \quad \text{for } x \in I_j \,.$$

Since the piecewise-constant reconstruction (4.5) is an order-preserving operation, it follows that $\bar{E}_h$ is likewise order preserving as a composition of 3 such operations; consequently the scheme is monotone.

The second-order accurate MUSCL scheme of van Leer [23] is (4.3) with the piecewise-linear reconstruction

$$(4.6a) \qquad R(x;\,\bar{w}) = \bar{w}_j + (x - y_j) \cdot s_j \qquad \text{for } x \in I_j \,,$$

where s_j is defined by

$$(4.6b) \qquad s_j = m\,(\Delta_{j-1/2}\bar{w}\,/\Delta_{j-1/2}\,y\;,\;\Delta_{j+1/2}\bar{w}/\Delta_{j+1/2}\,y)\;;$$

here y_j denotes the center of I_j . It is easy to verify that the particular form of the slope s_j in (4.6) implies that

$$\text{(4.7a)} \qquad TV\ (R\ (\cdot\ ;\ \bar{w})) = TV\ (\bar{w}) \quad ;$$

hence it follows from (4.4) that the scheme is TVD, i.e.,

$$\text{(4.7b)} \qquad TV\ (\bar{E}_h \cdot \bar{w}) \leq TV\ (\bar{w}) \ .$$

To simplify our presentation, we assume from now on that the partition $\{I_j^{\ n}\}$ is stationary and uniform, i.e.

$$\text{(4.8)} \qquad I_j^{\ n} = (x_{j-1/2}, x_{j+1/2}) \quad ;$$

this enables us to express the schemes (4.3) by standard grid notations.

The Godunov-type scheme (4.3) generates discrete values $\{v_j^{\ n}\}$, which are r-th order accurate approximations to $\{\bar{u}_j^{\ n}\}$, the cell-averages of the exact solution. We note, however, that the operation of the scheme (4.3) also involves a globally defined pointwise approximation to u(x,t) of the same order of accuracy which we denote by $v_h(x,t)$. The latter is defined for all x in the time-strips $t_n \leq t < t_{n+1}$ by

$$\text{(4.9)} \qquad v_h\ (\cdot, t_n + t) - E(t) \cdot R(\cdot\ ;\ v^n) \text{ for } \quad 0 \leq t < \tau \ .$$

We remark that (4.3) is the abstract operator expression of a scheme in the standard conservation form

$$(4.10a) \qquad v_j^{n+1} = v_j^n - \lambda\,(\bar{f}_{j+1/2} - \bar{f}_{j-1/2})$$

with the numerical flux

$$(4.10b) \qquad \bar{f}_{j+1/2} = \frac{1}{\tau}\int_0^\tau f(v_h\,(x_{j+1/2}, t_n + t))dt \quad .$$

For r = 1 (Godunov's scheme), the numerical flux (4.10b) can be expressed by (1.7). For $r \geq 2$, we make use of the fact that $v_h(x_{j+1/2}, t_n + t)$ in (4.10b) is needed only "in the small", in order to derive simple but adequate approximations to the numerical flux (see [16] for more details).

We remark that (4.7a) is sufficient but not a necessary condition for the scheme $\bar{E}_h$ to be TVD (4.7b). Other choices of the slope s_j in (4.6), such as

$$(4.6b)' \qquad h \cdot s_j = \bar{m}\,(\Delta_{j-1/2}\bar{w}, \Delta_{j+1/2}\bar{w})$$

or

$$(4.6b)'' \qquad h \cdot s_j = m\,(2\Delta_{j-1/2}\bar{w}\;, (\bar{w}_{j+1} - \bar{w}_{j-1})/2, 2\Delta_{j+1/2}\bar{w})$$

do not satisfy (4.7a); nevertheless the resulting scheme is TVD. This is due to the helping hand of the cell-averaging operator, which is not taken into account in (4.4).

MUSCL-type schemes, as all other TVD schemes, are second-order accurate only in the L_1-sense . In order to achieve higher-order of accuracy, we have to weaken our control over the possible increase in total variation due to the reconstruction step. We do so by introducing the notion of essentially non-oscillatory (ENO) schemes in the next section.

5. ENO SCHEMES.

We turn now to describe the recently developed essentially non-oscillatory (ENO) schemes of [16], which can be made accurate to any finite order r . These are Godunov-type schemes (4.3) in which the reconstruction $R(x\ ;\ \bar{w})$, in addition to relations (4.2), also satisfies

$$\text{(5.1)} \qquad TV\ (R(\ \cdot\ ;\ \bar{w})) \leq TV\ (\bar{w}) + O(h^{1+p})\ ,\ p > 0$$

for any piecewise-smooth function $w(x)$. Such a reconstruction is essentially nonoscillatory in the sense that it may not have a Gibbs-like phenomenon at jump-discontinuities of $w(x)$, which involves the generation of $O(1)$ spurious oscillations (that are proportional to the size of the jump); it can, however, have small spurious oscillations which are produced in the smooth(er) part of $w(x)$, and are usually of the size $O(h^r)$ of the reconstruction error (4.2a).

When we use an essentially non-oscillatory reconstruction in a Godunov-type scheme, it follows from (4.4) and (5.1) that the resulting scheme (4.3) is likewise essentially nonoscillatory (ENO) in the sense that for all piecewise-smooth functions $w(x)$

$$\text{(5.2)} \qquad TV\ (\bar{E}_h \cdot \bar{w}) \leq TV\ (\bar{w}) + O(h^{1+p})\ ,\ p>0\ \ ;$$

i.e., it is "almost TVD". Property (5.2) makes it reasonable to believe that at time $t = T$, after applying the scheme $N = T/\tau = O(h^{-1})$ times, we can expect

$$\text{(5.3)} \qquad TV\ (v_h\ (\cdot\ ,\ T)) \leq C \cdot TV\ (u_o) + O(h^p)\ .$$

We recall that by Theorem 3.1, this implies that the scheme is convergent (at least in the sense of having convergent subsequences). This hope is supported by a very large number of numerical experiments. In order to conclude from (5.2) that for all $n > 0$,

$$TV\ (v^{n+1}) < TV\ (v^n) + 0(h^{1+p}),\ p>0 \tag{5.3}$$

we still have to show that, starting from a piecewise-smooth $u_o(x)$ in (4.3b), v^n remains sufficiently close in its regularity to a piecewise-smooth function, so that (5.2) applies to the following time-steps as well. Unfortunately, we have not been able as yet to analyze the regulatirty of v^n .

Next we describe one of the techniques to obtain an ENO reconstruction. Given cell-averages $\{\bar{w}_j\}$ of a piecewise smooth function w(x), we observe that

$$h\ \bar{w}_j = \int_{x_{j-1/2}}^{x_{j+1/2}} w(y)dy = W(x_{j+1/2}) - W(x_{j-1/2}) \tag{5.4a}$$

where

$$W(x) = \int_{x_o}^{x} w(y)dy \tag{5.4b}$$

is the primitive function of w(x). Hence we can easily compute the <u>point values</u> $\{W(x_{i+1/2})\}$ by summation

$$W(x_{i+1/2}) = h \sum_{j=i_o}^{i} \bar{w}_j \ . \tag{5.4c}$$

Let $H_m(x\ ;\ u)$ be an interpolation of u at the points $\{y_j\}$, which is accurate to order m, i.e.

$$(5.5a) \qquad H_m\,(y_j\ ;\ u) = u(y_j),$$

$$(5.5b) \qquad \frac{d^\ell}{dx^\ell} H_m\,(x\ ;\ u) = \frac{d^\ell}{dx^\ell}\, u(x) + O(h^{m+1-\ell}), \qquad 0<\ell<m.$$

We obtain our "reconstruction via primitive function" technique by defining

$$(5.6) \qquad R\,(x;\ \bar{w}) = \frac{d}{dx} H_r(x\ ;\ W).$$

Relation (4.2a) follows immediately from (5.5b) with $\ell = 1$ and the definition (5.4) , i.e.,

$$R(x\ ;\ \bar{w}) = \frac{d}{dx} H_r(x\ ;\ W) = \frac{d}{dx}\, W(x) + O(h^r)$$

$$= \ w(x) + O(h^r)$$

Relation (4.2b) is a direct consequence of (5.5a) and (5.4), i.e.,

$$A(I_j)\ R(\cdot\ ;\ \bar{w}) = \frac{1}{h} \int_{x_{j-1/2}}^{x_{j+1/2}} \frac{d}{dx} H_r(x,\ W)\ dx$$

$$= \frac{1}{h}\,[H_r(x_{j+1/2}\ ;\ W) - H_r(x_{j-1/2};\ W)] = \frac{1}{h}\,[W(x_{j+1/2}) - W(x_{j-1/2})] = \bar{w}_j .$$

To obtain an ENO reconstruction, we take H_r in (5.6) to be the new ENO interpolation technique of the author [9]. In this case, $H_m(x\ ;\ u)$ is a piecewise-polynomial function of x of degree m, which is defined (omitting the u dependence) by

$$\text{(5.7a)} \qquad H_m(x\ ;\ u) = q_{j+1/2}(x) \qquad \text{for } y_j < y < y_{j+1}$$

where $q_{j+1/2}$ is the unique polynomial of degree m that interpolates u at the m+1 points

$$\text{(5.7b)} \qquad S_m(i) \equiv \{y_{i+1}, \ldots, y_{i+m}\}$$

for a particular choice of $i = i(j)$ (to be described in the following). To satisfy (5.5a), we need

$$q_{j+1/2}(y_j) = u(y_j)\ ,\ q_{j+1/2}(y_{j+1}) = u(y_{j+1})\quad ;$$

therefore, we limit our choice of i(j) to

$$\text{(5.7c)} \qquad j - m+1 < i(j) < j\ .$$

The ENO interpolation technique is nonlinear: At each interval $[y_j, y_{j+1}]$, we consider the m possible choices of stencils (5.7b) subject to the restriction (5.7c), and assign to this interval the stencil in which u is "smoothest" in some sense; this is done by specifying i(j) in (5.7b).

The information about the smoothness of u can be extracted from a table of divided differences. The k-th divided difference of u

(5.8a) $$u[y_i, y_{i+1}, \dots, y_{i+k}] \equiv u[S_k(i)]$$

is defined inductively by

(5.8b) $$u[S_o(i)] = u(y_i)$$

and

(5.8c) $$u[S_k(i)] = (u[S_{k-1}(i+1)] - u[S_{k-1}(i)])/(y_{i+k}-y_i).$$

If u(x) is m times differentiable in $[y_i, y_{i+m}]$ then

(5.9a) $$u[S_m(i)] = \frac{1}{m!}\, u^{(m)}(\xi)\ , \text{ for some } y_i < \xi < y_{i+m}$$

If $u^{(p)}(x)$ has a jump discontinuity in $[y_i, y_{i+m}]$ then

(5.9b) $$u[S_m\,(i)] = O(h^{-m+p}[u^{(p)}]\ ),\ 0 < p < m-1$$

($[u^{(p)}]$ in the RHS of (5.9b) denotes the jump in the p-th derivative).

Relations (5.9) show that $|u[S_m(i)]|$ is a measure of the smoothness of u in S_m (i), and therefore can serve as a tool to compare the relative smoothness of u in various stencils. The simplest algorithm to assign $S_m(i(j))$ to the interval $[y_j, y_{j+1}]$ is the following:

<u>Algorithm I.</u> Choose $i(j)$ so that

(5.10) $$|u[S_m(i(j))]| = \min_{j-m+1 \leq i \leq j} \{|u[S_m(i)]|\} .$$

Clearly (5.10) selects the "smoothest" stencil, provided that h is sufficiently small (but not smaller than the round-off error of the machine would permit!).

In order to make a sensible selection of stencil also in the "pre-asymptotic" case, we prefer to use the following hierarchial algorithm:

<u>Algorithm II:</u> Let $i_k(j)$ be such that $S_k(i_k(j))$ is our choice of a (k+1)-point stencil for $[y_j, y_{j+1}]$. Obviously we have to set

(5.11a) $$i_1(j) = j$$

To choose $i_{k+1}(j)$, we consider as candidates the two stencils

(5.11b) $$S^L_{k+1} = S_{k+1}(i_k(j) - 1) \quad ,$$

(5.11c) $$S^R_{k+1} = S_{k+1}(i_k(j)) ,$$

which are obtained by adding a point to the left of (or to the right of) $S_k(i_k(j))$, respectively. We select the one in which u is relatively smoother, i.e.,

(5.11d) $$i_{k+1}(j) = \begin{cases} i_k(j) - 1 & \text{if } |u[S^L_{k+1}]| < |u[S^R_{k+1}]| \\ i_k(j) & \text{otherwise.} \end{cases}$$

Finally we set $i(j) = i_m(j)$.

Using Newton's form of interpolation, we see that the polynomials $\{q_k(x)\}$, $1 \leq k \leq m$, corresponding to the stencils $S^k = S_k(i_k(j))$ selected by Algorithm II, satisfy the relation

$$q_{k+1}(x) = q_k(x) + u[S^{k+1}] \prod_{y \in S^k}(x-y) \, . \tag{5.11e}$$

This shows that the choice made in (5.11d) selects q_{k+1} to be the one that deviates the least from q_k. It is this property that makes Algorithm II meaningful also for h in the pre-asymptotic range.

In Figure 3, we apply the piecewise polynomial interpolation (5.7) to a piecewise-smooth function u which has in $[-1,1]$ 3 jump discontinuities in the function itself and another one in the first derivative. This function is shown in Figure 3 by a continuous line on which there are 30 circles that denote the values used for the interpolation. This function was continued periodically outside $[-1,1]$ (not shown in the picture).

In Figure 3a, we show the 6-th order polynomial (5.7) (i.e., $m = 6$) with the *predetermined* stencil $i(j) = j$; i.e., the 7-points stencil $\{y_j, y_{j+1}, \ldots, y_{j+6}\} = S_6(j)$ is used to define $q_{j+1/2}$ in $[y_j, y_{j+1}]$. Figure 3a shows a highly oscillatory behavior of the interpolation polynomial.

In Figure 3b, we show the same 6-th order polynomial (5.7) except that now we use the *adaptive* stencil which is selected by Algorithm II (5.11).

To understand why this interpolation works as well as it does, we consider the following two possibilities:

(i) $[y_j, y_{j+1}]$ is in the smooth part of u: For h sufficiently small, both Algorithms I and II choose a stencil $S_m(i(j))$ which is also in the smooth part of the function. In this case, (5.5b) in

$[y_j, y_{j+1}]$ is the standard result for m-th order interpolation of a smooth function. We observe the $q_{j+1/2}$ need not be a monotone approximation to u in $[y_j, y_{j+1}]$; nevertheless, its total variation there cannot be more than $O(h^{m+1})$ larger than that of u.

(ii) $[y_j, y_{j+1}]$ contains a discontinuity: For h sufficiently small, the function u near $[y_j, y_{j+1}]$ can be thought of as a step-function. In the case of a step-function, the particular choice of i(j) is of no importance since all the stencils $S_m(i)$ with $j-m+1 \leq i \leq j$ lead to a $q_{j+1/2}(x)$ which is monotone in (y_j, y_{j+1}). This follows from the simple observation that in the case of a step-function, we have for all $1 \leq \ell \leq m$, except $\ell = j-i$

$$u(y_{i+\ell}) = u(y_{i+\ell+1}) \,, \tag{5.12a}$$

and, consequently, also

$$q_{j+1/2}(y_{i+\ell}) = q_{j+1/2}(y_{i+\ell+1}) \tag{5.12b}$$

Using Rolle's theorem, we count in (5.12b) (m-1) roots of $d\,q_{j+1/2}/dx$ outside (y_j, y_{j+1}). Since $dq_{j+1/2}/dx$ is a polynomial of degree (m-1), it follows that these are all its roots. Hence, $d\,q_{j+1/2}/dx$ does not vanish in (y_j, y_{j+1}), which shows that it is monotome there (see [17] and [15] for more details).

We conclude this section by showing in Figures 4 and 5 the solution to the shock-tube problem (2.7) by the ENO scheme with r = 2 (Figure 4) and r = 4 (Figure 5). Comparing Figures 4-5 to Figures 1-2, we observe a considerable improvement in performance (see [14] for more details).

6. NONLINEARITY, UPWIND DIFFERENCING AND LINEAR STABILITY.

In this section, we consider the constant coefficient case (2.1). In this case, the Godunov-type scheme (4.3) can be expressed as

$$(6.1a) \qquad v_j^{n+1} = \bar{R}(x_j - a\tau \; ; \; v^n) \quad ,$$

where $\bar{R}(x; \cdot)$ denotes the sliding average of R, i.e.,

$$(6.1b) \qquad \bar{R}(x; \cdot) = \frac{1}{h} \int_{-h/2}^{h/2} R(x+\xi \; ; \; \cdot)\, d\xi .$$

We note that since R is a piecewise polynomial of degree (r−1), $\bar{R}$ is a piecewise-polynomial of degree r. Moreover, the conservation property (4.2b) shows that $\bar{R}(x \; ; \; v^n)$ is an interpolation of $\{v_j^n\}$. It is interesting to note that using R which is obtained via the primitive function (5.6), we get from (6.1) the particularly simple form

$$(6.2a) \qquad v_j^{n+1} = \frac{1}{h} \; [H_r(x_{j+1/2} - a\tau; \; V^n) - H_r(x_{j-1/2} - a\tau; \; V^n)\;],$$

where $\{V_{j+1/2}^n\}$ is defined at $\{x_{j+1/2}\}$ by (5.4), i.e.,

$$(6.2b) \qquad V_{j+1/2}^n = h \sum_{i=i_o}^{j} v_i^n .$$

Relation(6.2) directly relates Godunov-type schemes to interpolation. Clearly, if the interpolation H_r is based on a fixed stencil, then the resulting scheme is linear; the nonlinearity of the ENO schemes stems from its adaptive selection of stencil.

When $r = 1$, $\bar{R}$ in (6.1b) is necessarily the piecewise-linear interpolation of $\{v_j^n\}$; consequently the "upwind shift" $(-a\tau)$ forces the scheme to be the first-order upwind scheme. We recall however that the stencil in the ENO scheme is chosen from considerations of smoothness which have nothing to do with the PDE; the "upwind shift" $(-a\tau)$ is only by one cell; consequently the resulting ENO scheme (6.2) for $r > 2$ need not be, and in general is not, "upwind".

We turn now to study the second order accurate ENO scheme ($r = 2$ in (6.1) - (6.2)). It is easy to see that this scheme is identical to the MUSCL-type scheme (4.6) with s_j defined by (4.6b)′. It is somewhat more surprising to find that the MUSCL-type scheme (in the constant coefficient case), is identical to the second order accurate modified-flux scheme (3.11) with the correspondence

$$(6.3) \qquad g_j = h\,\sigma(a)\,s_j .$$

Consequently, all these second-order accurate TVD schemes can be written as (6.1) with a piecewise-parabolic $\bar{R}(x;\, v^n)$. For $a < 0$, we get

$$(6.4a) \quad v_j^{n+1} = \bar{R}(x_j - a\tau;\, v^n) = v_j^n - \lambda\, a\, \Delta_{j+1/2}v^n + \tfrac{1}{2}\, a(1+\lambda a) \cdot (s_{j+1} - s_j) ,$$

which is obtained from taking the sliding-average of (4.6a).

We observe that when in (4.6b)′

$$(6.4b) \qquad h \cdot s_j = \Delta_{j+1/2}v^n, \quad h \cdot s_{j+1} = \Delta_{j+3/2}v^n$$

then (6.4a) is the second-order accurate upwind-differencing scheme. However, when in (4.6b)″

$$(6.4c) \qquad h \cdot s_j = \Delta_{j-1/2} v^n, \quad h \cdot s_{j+1} = \Delta_{j+1/2} v^n$$

then (6.4a) is the central-differencing Lax-Wendroff scheme.

Based on this observation, we see that the MUSCL-type scheme with s_j defined by (4.6b) or (4.6b)′ satisfies (6.4b) when, as a function of i,

$$(6.4b)' \qquad \{ |\Delta_{i+1/2} v^n| \} \text{ is decreasing,}$$

and it satisfies (6.4c) when

$$(6.4c)' \qquad \{ |\Delta_{i+1/2} v^n| \} \text{ is increasing.}$$

This shows that the "popular" reference to the MUSCL scheme and the modified flux scheme as "upwind differencing" schemes is not justified.

We remark that the scheme (6.4a) is second-order accurate only if

$$(6.5a) \qquad s_{j+1} - s_j = h\, u_{xx} + O(h^2) .$$

This shows that in addition to

$$(6.5b) \qquad s_j = u_x(x_j) + O(h)$$

we need also the Lipschitz-continuity of the O(h) term in (6.5b). As we have mentioned earlier, the MUSCL scheme, as well as the modified flux scheme and other TVD schemes, fail to have this extra smoothness at local extrema, which are the transition points between (6.4b) and (6.4c); consequently, their accuracy drops to first order at points of local extremum.

The analysis of these second-order accurate nonlinear schemes shows that the "nature" of the scheme depends on differences of its numerical solution; therefore, local linearization is not justified. Since the two schemes in (6.4) are linearly stable, such incorrect linearization would nevertheless result in a correct statement of stability. This is not the case for $r > 2$, where, as r increases, more and more of the various choices of stencil can be identified as if belonging to a linearly unstable scheme. Since Fourier analysis is valid only if the same stencil is used everywhere, this identification is not necessarily relevant and may actually be quite misleading.

A situation of this type is encountered when we consider the initial-boundary-value problem (IBVP) in $-1<x<1$

$$u_t + u_x = 0 \quad , \; u(x, 0) = u_o(x) \; , \; u(-1,t) = g(t); \tag{6.6}$$

$x = 1$ is an "outflow boundary" and no condition needs to be specified there. We divide $[-1,1]$ into $(J+1)$ interval $\{I_j\}_{j=0}^{J}$, where $I_j = (x_{j-1/2}, x_{j+1/2})$ and

$$x_{-1/2} = -1 \; , \; x_{J+1/2} = 1. \tag{6.7a}$$

Given cell averages $\{\bar{w}_j\}$ for $j = 0, \ldots, J$ we define $W(x_{-1/2}) = 0$ and compute $W(x_{j+1/2})$, $j = 1, \ldots, J$ by (5.4c) with $i_o = 0$; thus $W(x_{j+1/2})$ is given also at $x = \pm 1$. Next we evaluate $H_r(x; w)$ by Algorithm II, which is modified so that the choice of stencil in (5.11) is restricted to available data. Thus, $H_r(x;w)$ is defined for $-1 < x < 1$, and as before we define

$$\text{(6.6b)} \qquad R\ (x;\ \bar{w}) = \frac{d}{dx} H_r\ (x;\ w) \quad , \quad -1 < x < 1 \ .$$

Using this definition of $R(x; \bar{w})$ in $[-1,1]$, we modify the Godunov-type scheme (4.3) by

$$\text{(6.7a)} \qquad v_j^{n+1} = A(I_j) \cdot \tilde{E}(\tau) \cdot R(\cdot\ ;\ v^n) \qquad , \ 0 < j < J \ .$$

$$\text{(6.7b)} \qquad v_j^{o} = A(I_j) \cdot u_o \ .$$

Here $\tilde{v}\ (t) = \tilde{E}(t) \cdot R(\ \cdot\ ;\ v^n)$ is the solution in the small (i.e., for $0 < t < \tau$) of the IBVP

$$\text{(6.7c)} \qquad \tilde{v}_t + f(\tilde{v})_x = 0,\ \tilde{v}(x,0) = R(x;v^n)\ ,\ \tilde{v}(-1,t) = g(t_n + t).$$

This implementation of Godunov-type schemes to IBVP's is very convenient: There are no "artificial numerical boundaries", and the prescribed boundary conditions are handled on the level of the PDE (6.7c). We observe, however, that near $x = -1$ the scheme is "differenced against the wind", which is linearly unstable if done everywhere. Therefore, our experience with linear schemes may inhibit us from using this approach. Overcoming this inhibition, we have performed a large numbe of numerical experiments with the so modified ENO schemes (two of which are presented in the following) and we are happy to report that these schemes have been found to be stable in all our experiments.

In Table 1, we present a mesh-refinement chart for the IBVP (6.6) with

$$u(x,0) = \sin \pi x \ , \ u(-1,t) = -\sin \pi\ (1+t) \quad . \tag{6.8}$$

The ENO schemes were used with a CFL number of 0.8, and the results are shown at $t = 2$. Table 1 indicates that the ENO schemes with $1 \leq r \leq 6$ are convergent in this case; the accumulation of error seems to be linear. Comparing Table 1 to the periodic case (see [g]), we observe that the results for the IBVP are slightly better in the asymptotic range, which is to be expected.

Next we consider the IBVP (6.6) with

$$u(x,o) = e^{-x} \quad , \ u(-1,t) = e^{1+t} \ , \tag{6.9a}$$

the solution to which is

$$u(x,t) = e^{-x+t} \tag{6.9b}$$

We observe that: (i) $|u^{(k)}(x,t)|$ is a monotone decreasing function of x for all k and t. Consequently, if we apply Algorithm II to $\bar{u}(\cdot\ ,t)$ we get $i(j) = j$ in (5.11). (ii) The scheme (6.2) with the <u>fixed</u> choice $i(j) = j$ is linear and strongly "biased against the wind"; consequently, it is linearly unstable.

In Table 2, we present a mesh-refinement chart for the solution at $t = 1$ of the IBVP (6.9) by the 4-th order ENO scheme ($r = 4$ in (6.6) - (6.7)) with CFL = 0.4. In spite of the previous observations, we find that the scheme seems to be convergent. This "paradox" is resolved once we examine the data in Figures 6 and 7 for J = 80 and 160, respectively. In (a), (b), (c) and (d), we show the absolute value of the k-th divided difference $|v[S_k]|$ for $k = 0, 1, 2, 3$, respectively. We see that the numerical solution and its first divided difference are monotone. However, the second and third divided differences are oscillatory. This allows the scheme to select $i(j) \neq j$ in (5.11). The actual choice of $i(j)$ at $t = 1$ is shown in Figure 6e and Figure 7e; the straight line in these figures is $i(j) = j$. Comparing Figure 6d to Figure 7d, we see that the oscillations in $v[S_3]$, the third divided difference of v, are uniformly bounded under refinement. Analysis of the numerical data suggests that

(i) $\quad v\,[S_3] \xrightarrow{w} u^{(3)}(x,t)$ (in an average sense) as $h \to 0$;

(ii) $\quad v[S_k] = u^{(k)}(x,t) + O(h^{3-k})$ for $k=0, 1, 2$.

Finally, we consider the application of the 4-th order ENO scheme to the periodic IVP

(6.10a) $\quad u_t + u_x = 0, \quad u(x,0) = ???, \quad v_j^{\,o} = (-1)^j.$

We observe that the mesh oscillation data in (6.10a), (6.10b) $$v_j^{\,o} = (-1)^j = e^{-ij\Pi}$$

is the highest frequency in (2.3b), which determines the linear stability of the constant coefficient scheme (2.2). We note, however, that as h decreases, the total variation of v^o becomes unbounded. Consequently, v^o does not represent a BV function and, therefore, need not be considered when testing for total-variation-stability in (3.1). In the following, we describe numerical experiments where we apply the 4-th order ENO scheme to (6.10) anyhow. The selection of stencil (5.11) is designed to make a sensible choice only when applied to piecewise-smooth data. In the mesh-oscillation case $|v[S_k(i)]|$ is constant as a function of i for all k; consequently, (5.11) results in the arbitrary choice of the uniform stencil $i(j) = j-3$ (see Figure 8b). As in the previous case, the ENO scheme becomes a constant coefficient scheme (2.2) for which linear stability analysis applies. In Figure 8c, we show the amplification factor of the mesh-oscillation mode

(6.10c) $$g(\nu) = \sum_{\ell=-k}^{k} (-1)^{\ell} \, c_{\ell}(\nu)$$

as a function of the CFL number $\nu = \lambda a$. The amplification factor (6.10c) for the ENO schemes is determined by two competing factors: (i) Increase of oscillations due to the reconstruction, which is based on the highly-oscillatory interpolation of the mesh oscillation (6.10b); (ii) Decrease of oscillations due to the operation of cell-averaging on the translated data. Figure 8c shows that for $\nu < 0.26$, the latter wins and the scheme is linearly stable; for larger values of ν the scheme is linearly unstable. In Figures 8d and 8e, we show the numerical solution of the 4-th order ENO scheme with

$\nu = 0.6$ after a single time-step (n=1) and twenty time-steps (n=20), respectively. Clearly, the numerical solution blows up like $(1.67)^n$.

It is amusing to realize that this "linear instability" is itself "nonlinearly unstable" in the sense that any nonuniform perturbation of the mesh-oscillation data turns the ENO scheme into a stable nonlinear scheme. To demonstrate this point, we perturb the mesh-oscillation data by a random noise of the size 10^{-6} of the round-off error (see Figures 9a and 9b), and repeat the previous calculation. In Figures 9d - 9k, we present subsequent "snap-shots" of the numerical solution, which show that the numerical solution decays in both the amplitude and the number of oscillations; observe that the rate of decay is faster for the highly oscillatory components of the solution and slower for the smoother ones.

This property enables the scheme to combine "robustness" with accuracy. We demonstrate this feature of the ENO schemes in Figure 10 where we apply the 4-th order scheme with $\nu = 0.4$ to initial data of $\sin \pi x$ perturbed by random noise of the size 10^{-1}; the squares denote the numerical solution; the continuous line shows $\sin \pi x$.

Acknowledgement

I would like to thank Sukumar Chakravarthy, Bjorn Engquist and Stan Osher for various contributions to this research, and for making my stay at UCLA the pleasant and fruitful period that it was.

This research was supported by NSF Grant No. DMS85-03294, ARO Grant No. DAAG29-85-K0190, and NASA Consortium Agreement No. NCA2-IR390-403. The author was supported by NASA Contracts NAS1-17070 and NAS1-18107 while in residence at ICASE.

References

[1] Boris, J. P. and D. L. Book, "Flux corrected transport. I. SHASTA, a fluid transport algorithm that works," J. Comp. Phys., Vol. 11 (1973), pp. 38-69.

[2] Colella, P. and P. R. Woodward, "The piecewise-parabolic method (PPM) for gas-dynamical simulations," J. Comp. Phys., Vol. 54 (1984), pp. 174-201.

[3] Crandall, M. G. and A. Majda, "Monotone difference approximations for scalar conservation laws," Math. Comp., Vol. 34 (1980), pp. 1-21.

[4] Glimm, J., "Solutions in the large for nonlinear hyperbolic systems of equations," Comm. Pure Appl. Math., Vol. 18 (1965), pp. 697-715.

[5] Godunov, S. K., "A difference scheme for numerical computation of discontinuous solutions of equations of fluid dynamics," Math. Sbornik, Vol. 47 (1959), pp. 271-306. (in Russian)

[6] Harten, A., "The artificial compression method for computation of shocks and contact-discontinuities: III. Self-adjusting hybrid schemes," Math. Comp., Vol. 32 (1978) pp. 363-389.

[7] Harten, A., "High resolution schemes for hyperbolic conservation laws," J. Comp. Phys., Vol. 49 (1983), pp. 357-393.

[8] Harten, A., "On a class of high resolution total-variation-stable finite-difference schemes," SINUM, Vol. 21 (1984), pp. 1-23.

[9] Harten, A., "On high-order accurate interpolation for non-oscillatory shock capturing schemes," MRC Technical Summary Report #2829, University of Wisconsin, (1985).

[10] Harten, A. and J. M. Hyman, "A self-adjusting grid for the computation of weak solutions of hyperbolic conservation laws," J. Comp. Phys., Vol. 50 (1983), pp. 235-269.

[11] Harten, A., J. M. Hyman and P. D. Lax, "On finite-difference approximations and entropy conditions for shocks," Comm. Pure Appl. Math., Vol. 29 (1976), pp. 297-322.

[12] Harten, A. and P. D. Lax, "A random choice finite-difference scheme for hyperbolic conservation laws," SIAM J. Numer. Anal., Vol. 18 (1981), pp. 289-315.

[13] Harten, A., P. D. Lax and B. van Leer, "On upstream differencing and Godunov-type schemes for hyperbolic conservation laws," SIAM Rev., Vol. 25 (1983), pp. 35-61.

[14] Harten, A. and S. Osher, "Uniformly high-order accurate non-oscillatory schemes, I.," MRC Technical Summary Report #2823, May 1985, to appear in SINUM.

[15] Harten, A., B. Engquist, S. Osher and S. R. Chakravarthy, "Uniformly high-order accurate non-oscillatory schemes, II." (in preparation)

[16] Harten, A., B. Engquist, S. Osher and S. R. Chakravarthy, "Uniformly high-order accurate non-oscillatory schemes, III," ICASE Report No. 86-22 (April 1986).

[17] Harten, A., S. Osher, B. Engquist and S. R. Chakravarthy, "Some results on uniformly high-order accurate essentially non-oscillatory schemes," in "Advances in Numerical and Applied Mathematics, J. C. South, Jr. and M. Y. Hussaini (eds.), ICASE Report No. 86-18, (March 1986); also to appear in J. App. Num. Math.

[18] Jameson, A. and P. D. Lax, in "Advances in numerical and applied mathematics," J. C. South, Jr. and M. Y. Hussaini (eds.) (1986), ICASE Report No. 86-18; also to appear in J. App. Num. Math.

[19] Lax, P. D., "Weak solutions of nonlinear hyperbolic equations and their numerical computation," Comm. Pure Appl. Math., Vol. 7 (1954) pp. 159-193.

[20] Lax, P. D., "Hyperbolic systems of conservation laws and the mathematical theory of shock waves," Society for Industrial and Applied Mathematics, Philadelphia (1972).

[21] Lax, P. D. and B. Wendroff, "Systems of conservation laws," Comm. Pure Appl. Math., Vol. 13 (1960), pp. 217-237.

[22] van Leer, B., "Towards the ultimate conservative difference scheme. II. Monotonicity and conservation combined in a second order scheme," J. Comp. Phys., Vol. 14 (1974), pp. 361-370.

[23] van Leer, B., "Towards the ultimate conservative difference schemes V. A second order sequel to Godunov's method," J. Comp. Phys., Vol. 32 (1979), pp. 101-136.

[24] MacCormack, R. W., "Numerical solution of the interaction of a shock wave with a laminar boundar layer (Proc. 2nd Internat. Conf. on Numerical Methods in Fluid Dynamics, M. Holt (ed.), Lecture Notes in Phys., Vol. 8 (1970), Springer-Verlag, New York, pp. 151-163.

[25] Majda, A. and S. Osher, "Numerical viscosity and entropy condition," Comm. Pure Appl. Math., Vol. 32 (1979), pp. 797-838.

[26] Murman, E. M., "Analysis of embedded shock waves calculated by relaxation methods," AIAA J., Vol. 12 (1974), pp. 626-633.

[27] Osher, S. and S. R. Chakravarthy, "High-resolution schemes and the entropy condition," SINUM, Vol. 21 (1984), pp. 955-984.

[28] Osher, S. and E. Tadmor, "On the convergence of difference approximations to conservation laws," submitted to Math Comp.

[29] Richtmyer, R. D. and K. W. Morton, "Difference methods for initial value problems," 2nd ed., Interscience-Wiley, New York (1967).

[30] Roe, P.L., "Some contributions to the modeling of discontinuous flows." in Lectures in Applied Mathematics, Vol. 22 (1985), pp. 163-193.

[31] Sweby, P.K., "High resolution schemes using flux limiters for hyperbolic conservation laws," SINUM, Vol. 21 (1984), pp. 995-1011.

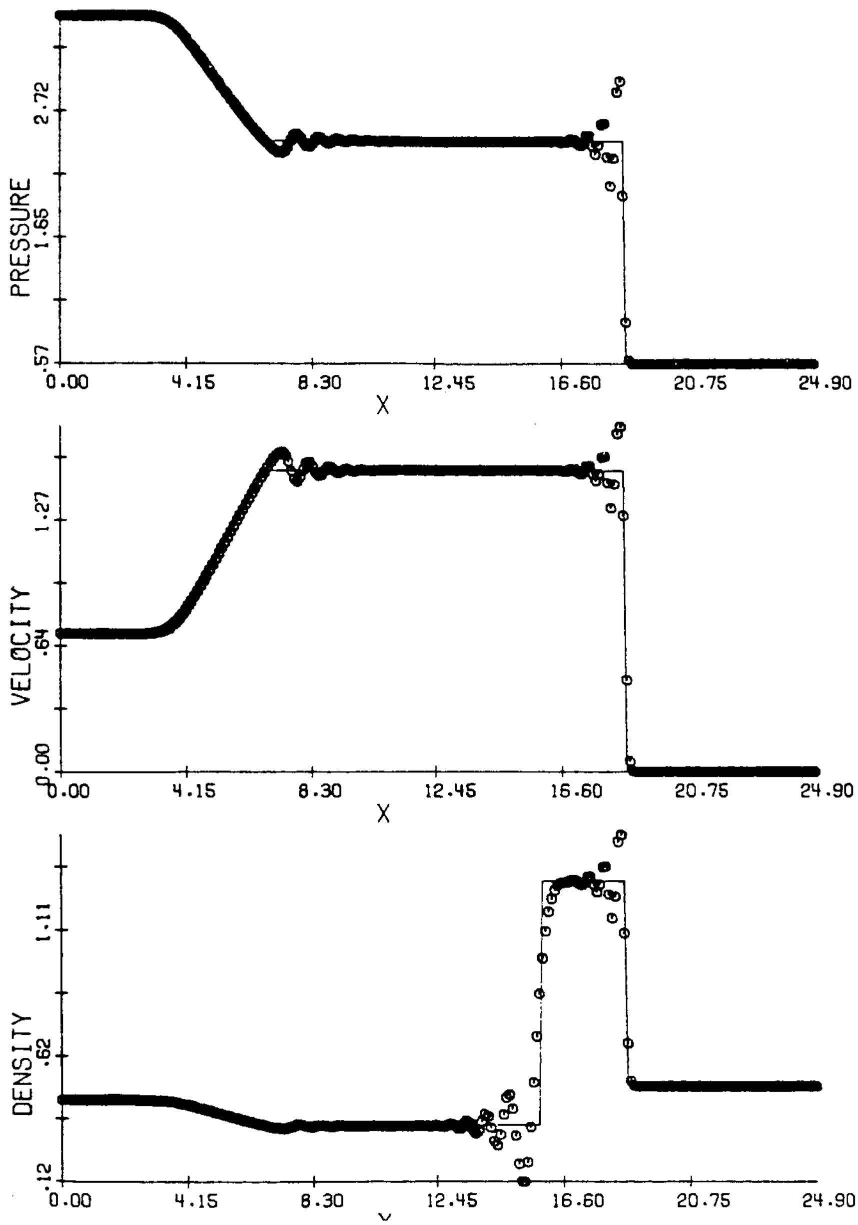

Figure 1. MacCormack scheme.

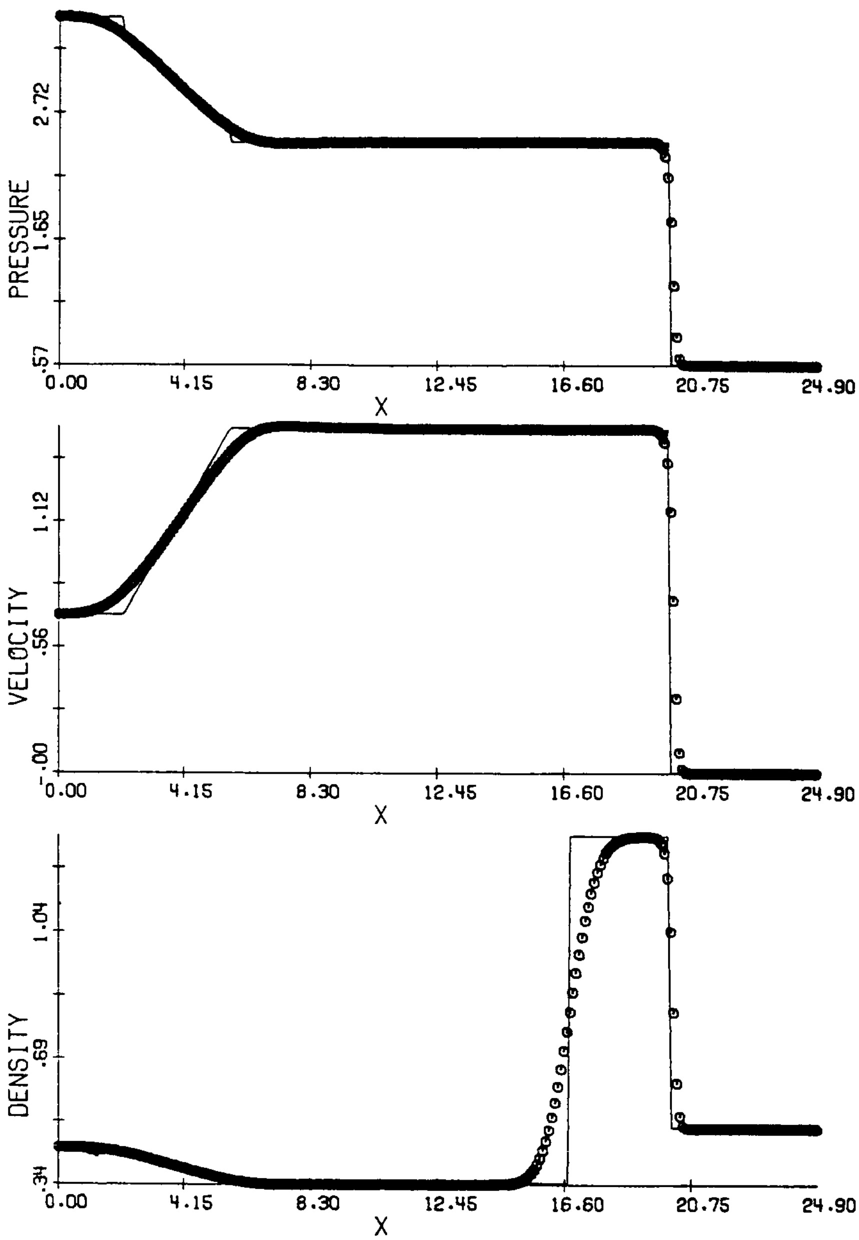

Figure 2. The first order scheme.

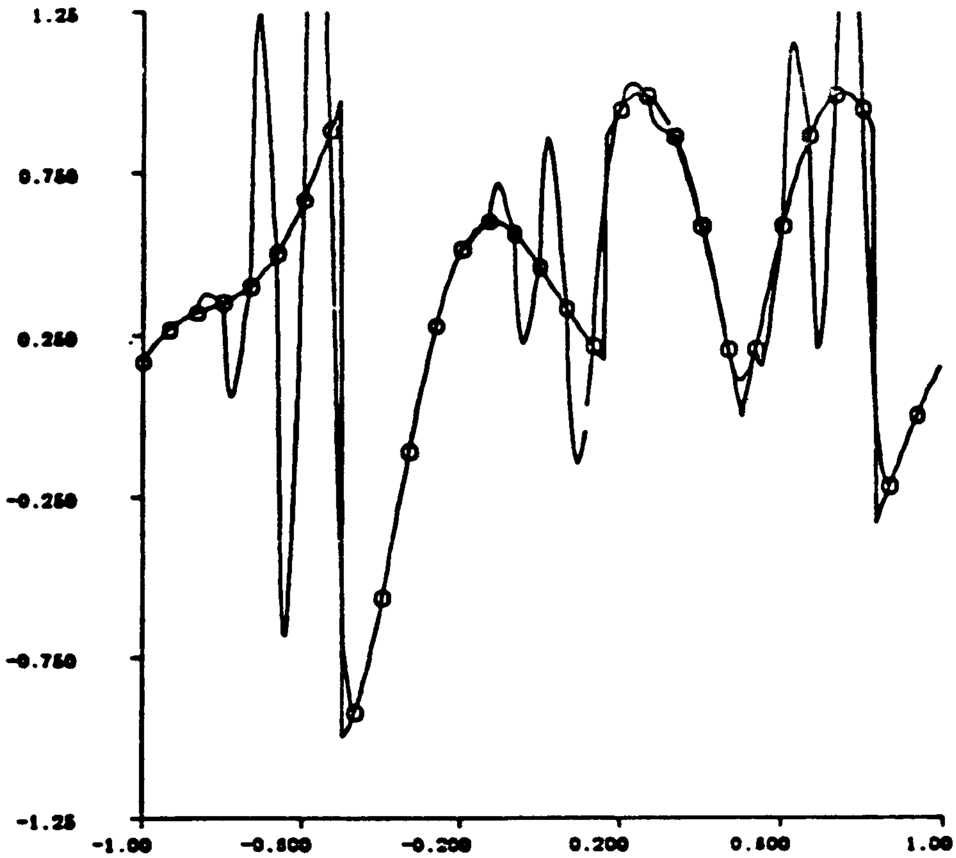

Figure 3a. H_6 (x:u) with a fixed stencil i(j) = j.

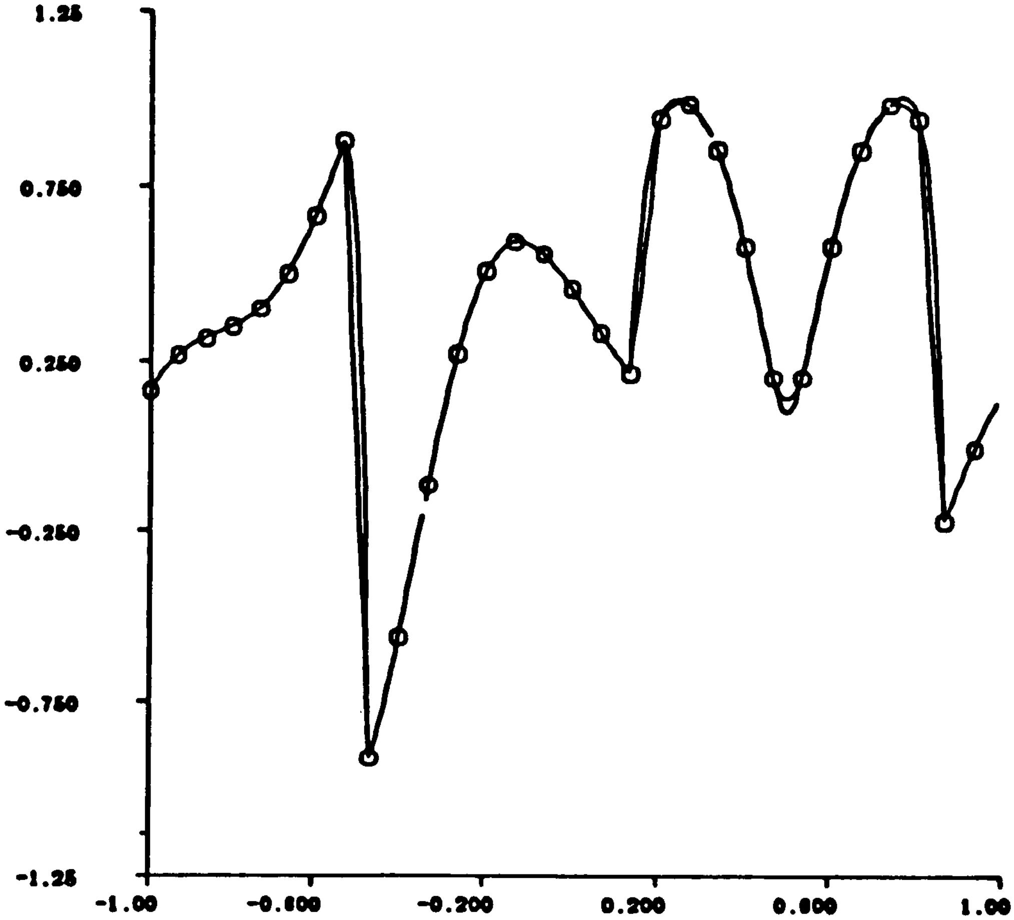

Figure 3b. H_6 (x;U) with an adaptive stencil (Algorithm II).

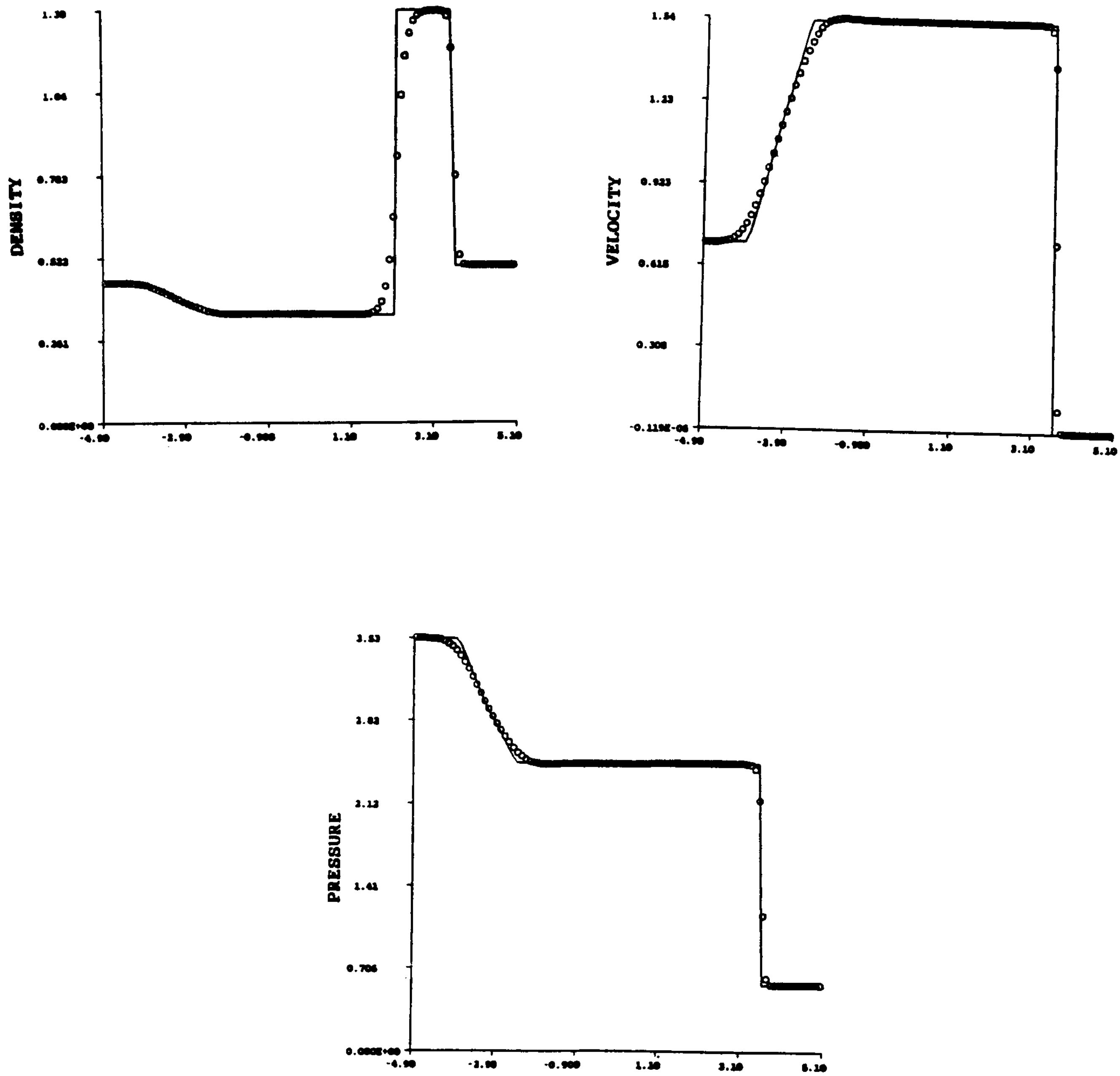

Figure 4. Second order ENO scheme.

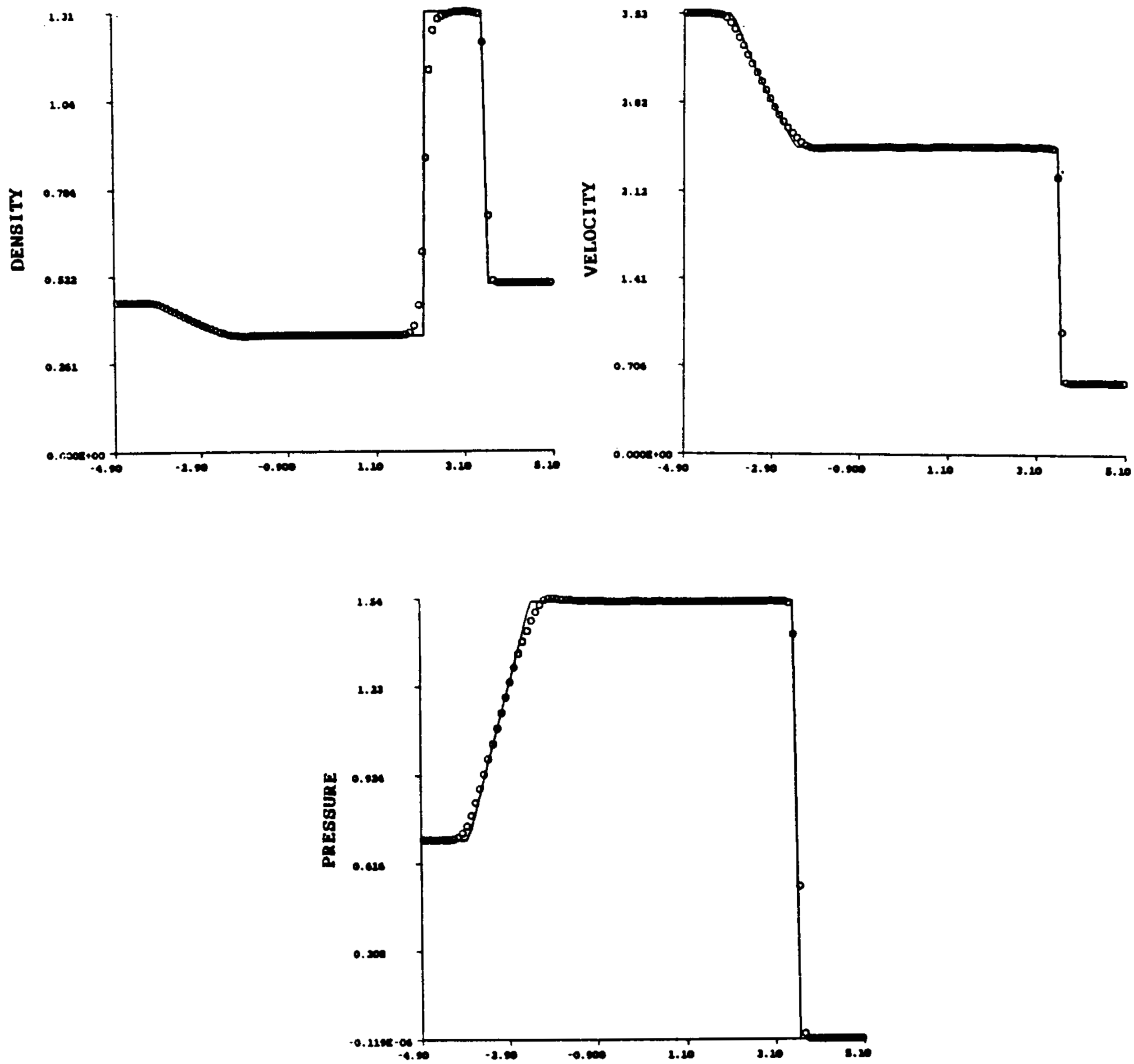

Figure 5. Fourth order ENO scheme.

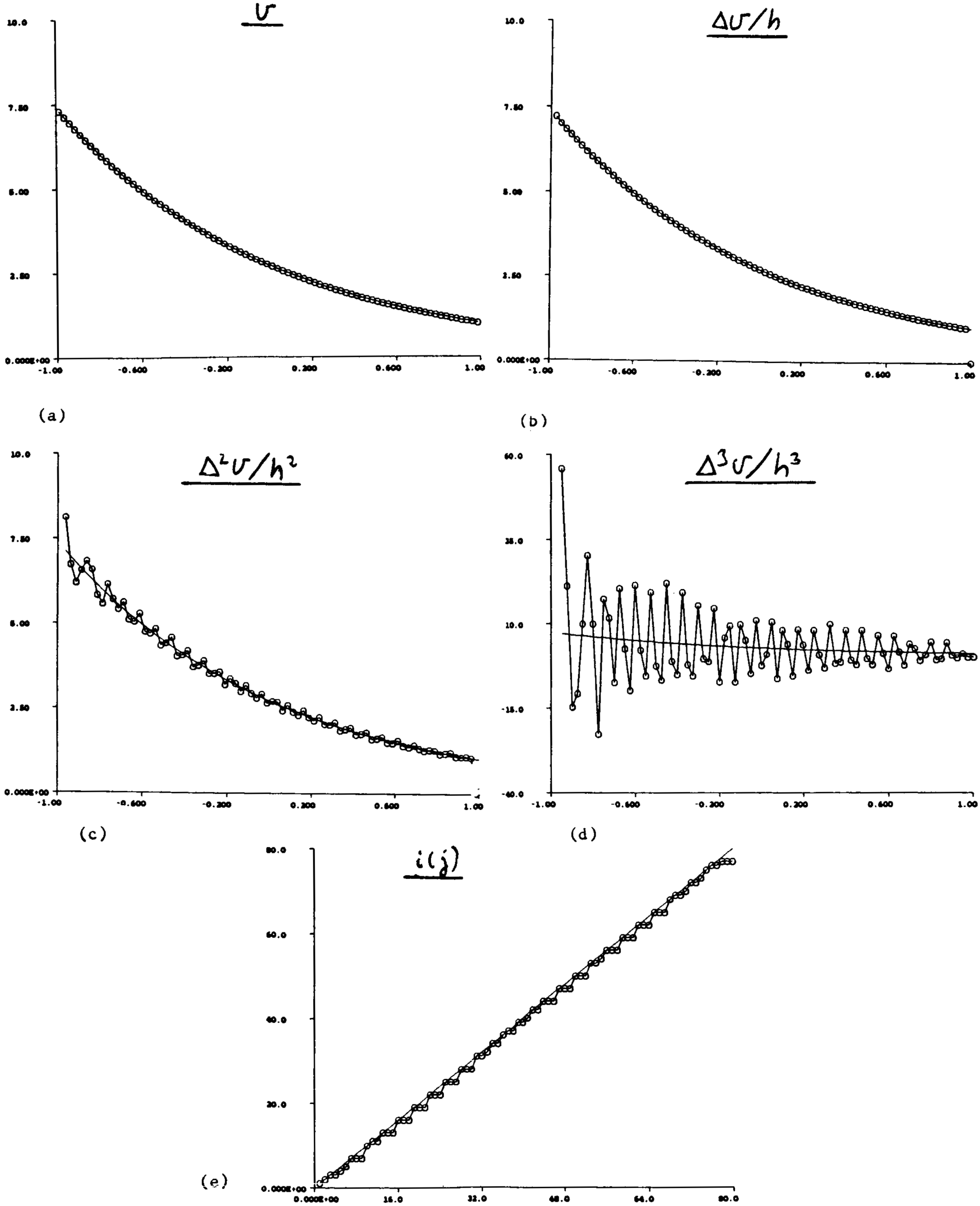

Figure 6. Solution of the IBVP (6.9)
at t=1 with I=80.

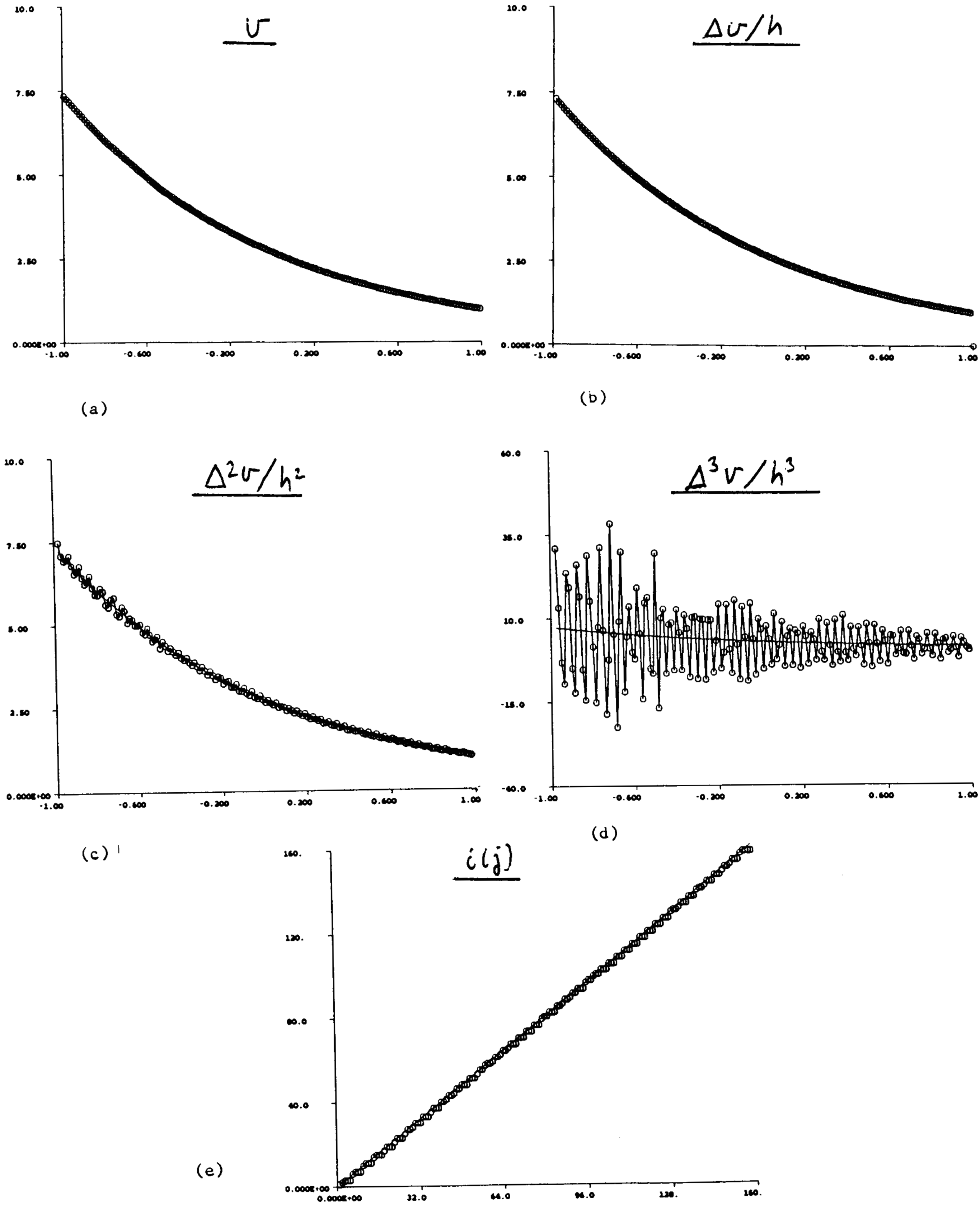

Figure 7. Solution of the IBVP (6.9) at t=1 with J=160.

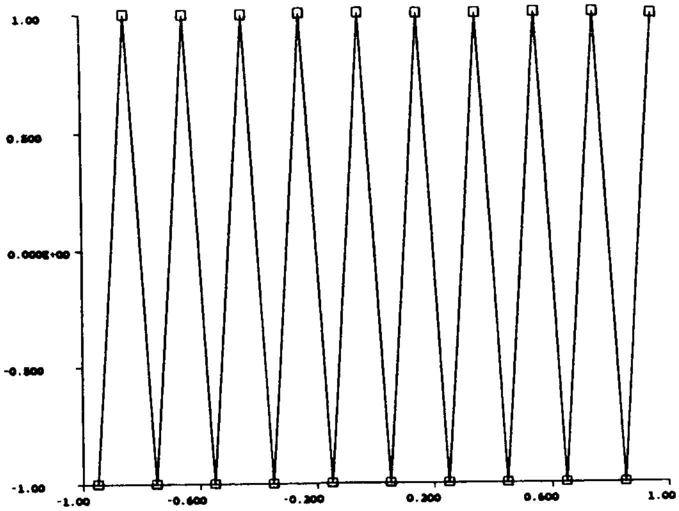

(a) n = 0

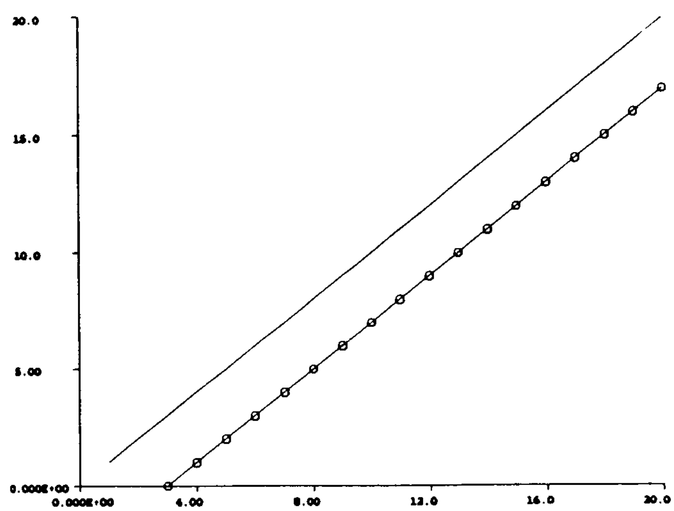

(b) i(j)

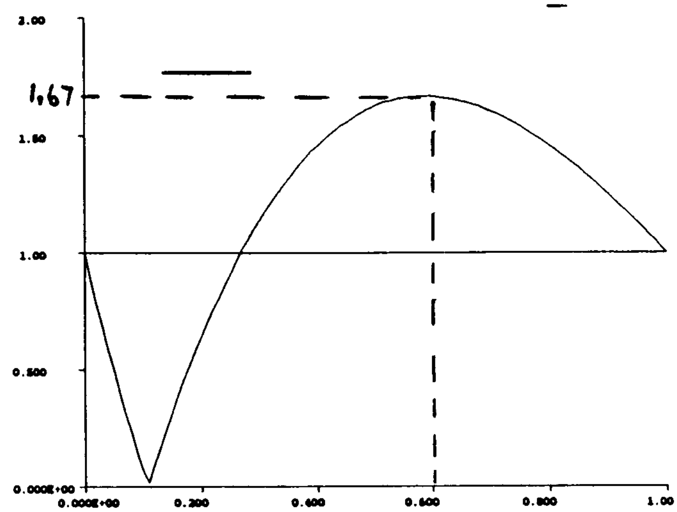

(c) g(ν)

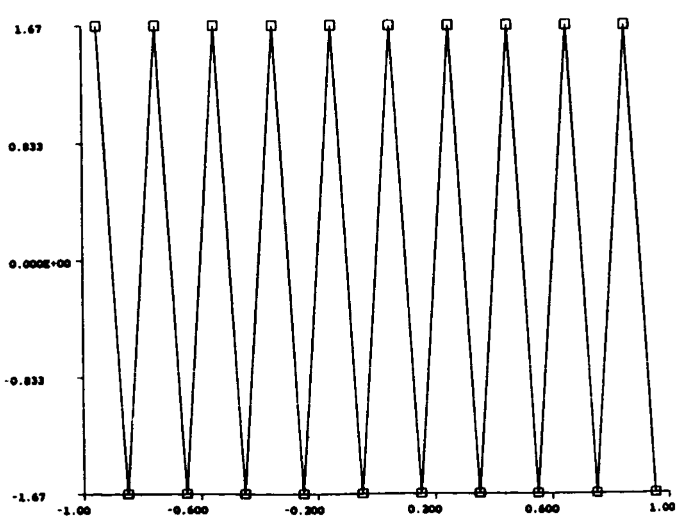

(d) n = 1 (max=-min=1.67

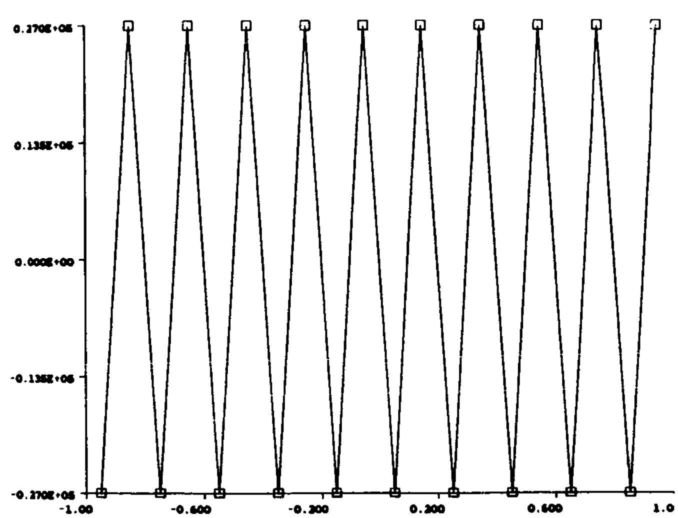

(e) n = 20 (max=-min=2.7×10^4)

Figure 8. Mesh-oscillation initial data.

n= 20 l= 0 time= 0.000E+00 dt=
cfl= 0.600 ni= 4
eps= 0.100E-05

j	$i(j)$	x	$u_0(x)$
7	6	-0.950	-.9999999E+00
8	7	-0.850	0.1000000E+01
9	7	-0.750	-.9999991E+00
10	7	-0.650	0.1000000E+01
11	11	-0.550	-.1000000E+01
12	11	-0.450	0.9999993E+00
13	11	-0.350	-.9999991E+00
14	11	-0.250	0.1000001E+01
15	15	-0.150	-.1000001E+01
16	15	-0.050	0.9999993E+00
17	15	0.050	-.9999996E+00
18	15	0.150	0.1000001E+01
19	19	0.250	-.9999997E+00
20	20	0.350	0.1000001E+01
21	20	0.450	-.9999995E+00
22	20	0.550	0.9999996E+00
23	20	0.650	-.1000000E+01
24	21	0.750	0.1000000E+01
25	25	0.850	-.1000001E+01
26	26	0.950	0.9999993E+00

(a) Initial data (numerical values)

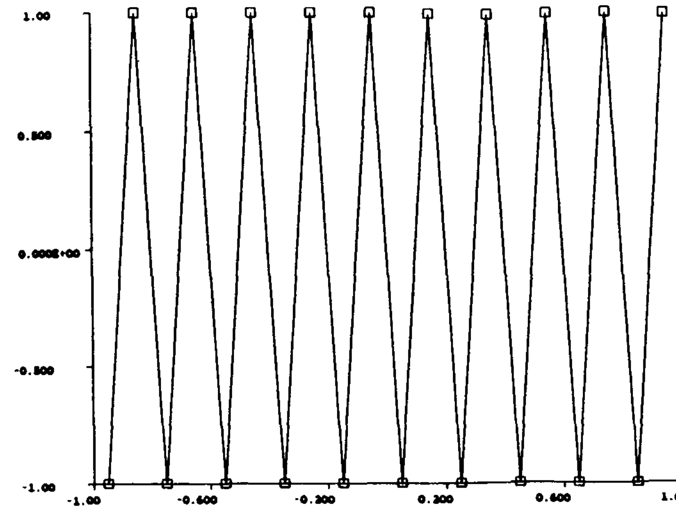

(b) $u_0(x)$ (n=0)

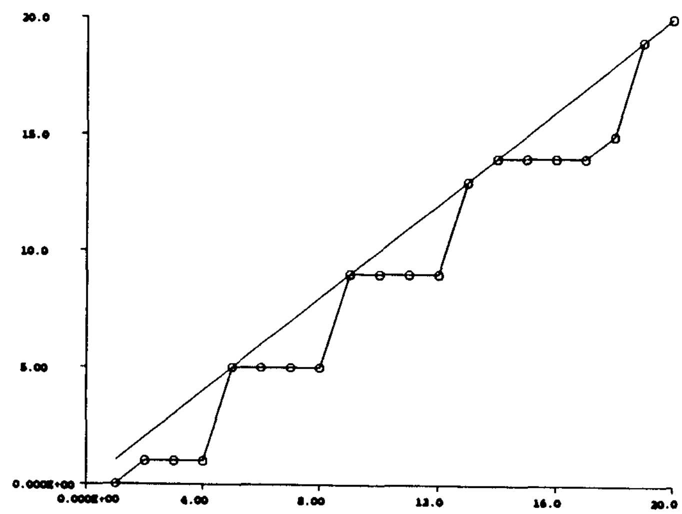

(c) $i(j)$

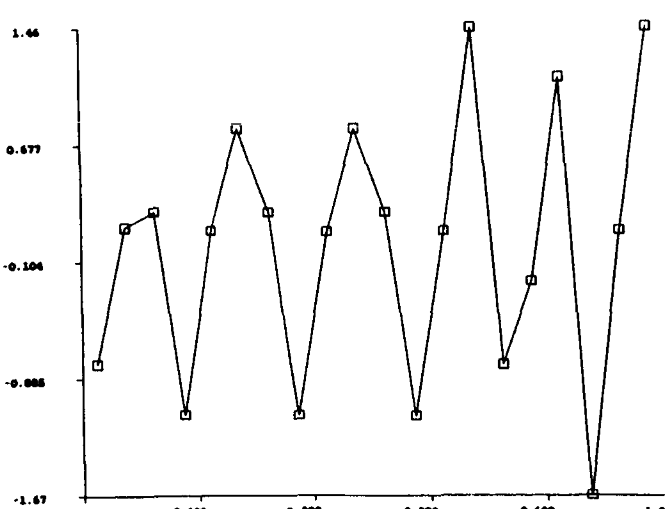

(d) n=1 (max-1.46, min--1.67)

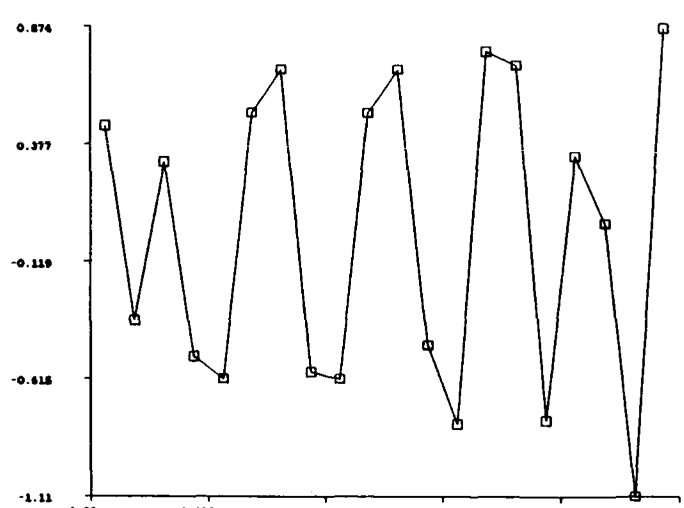

(e) n=2 (max=0.174, min=-1.11)

Figure 9. Randomly perturbed mesh-oscillation

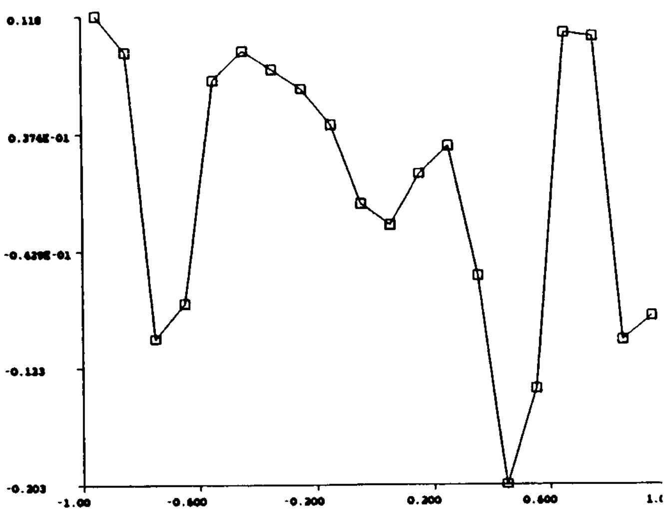

(f) n=20 (max=0.118, min=-0.203)

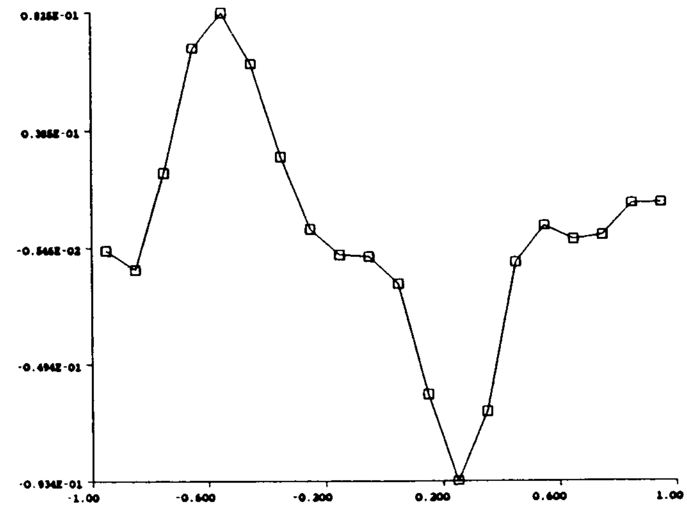

(g) n=50 (max=0.0825, min=-0.0934)

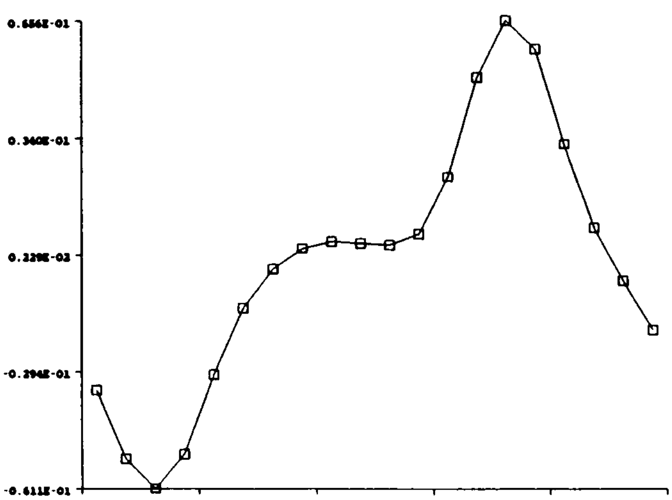

(h) n=1-- (max=0.0656, min=-0.0611)

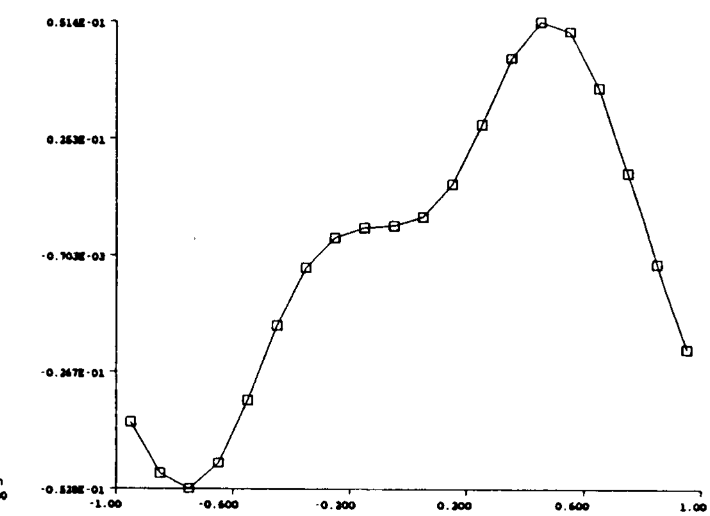

(i) n=200 (max=0.0514, min=-0.0528)

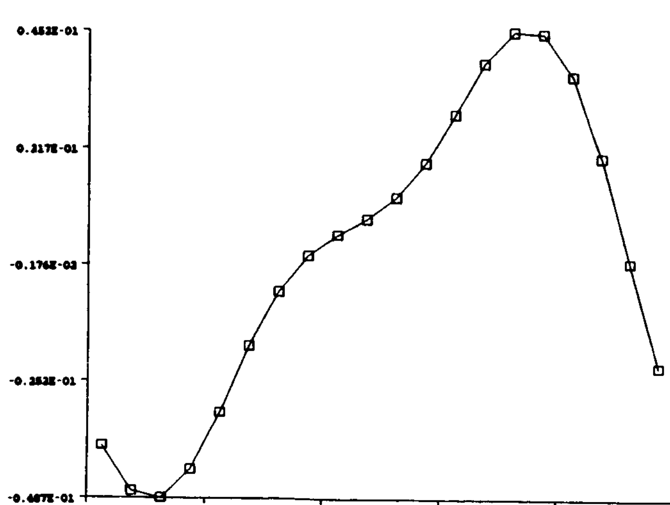

(j) n=400 (max=0.0452, min=-0.0487)

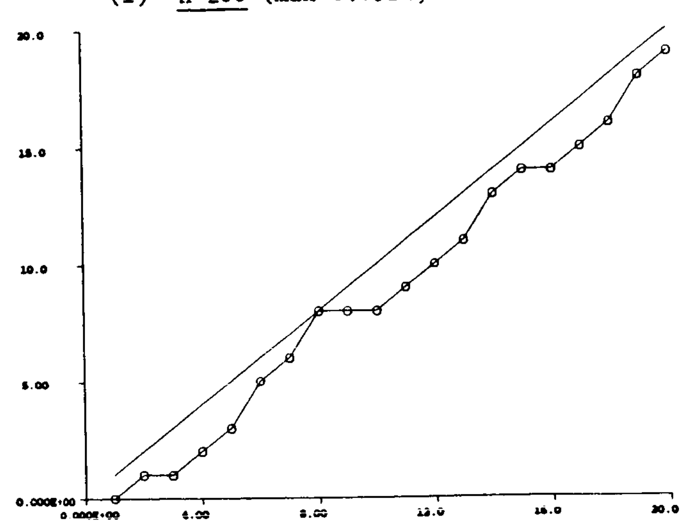

(k) i(j) for n=400

Figure 9. Continued

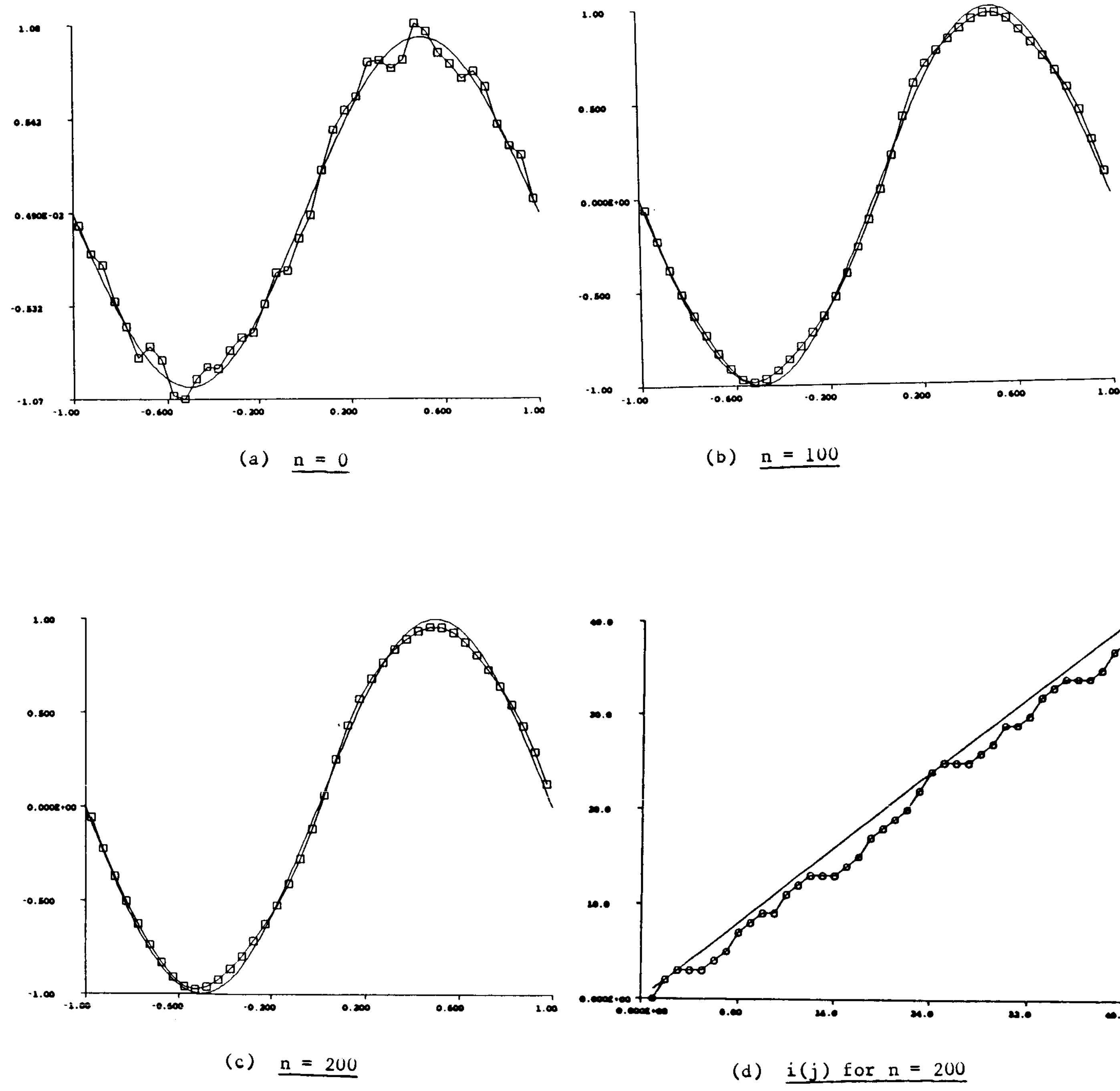

(a) n = 0

(b) n = 100

(c) n = 200

(d) i(j) for n = 200

Figure 10. Initial data of randomly perturbed sin (πx).

Table 1. Mesh-Refinement for ENO Schemes (IBVP)

$u_t + u_x = 0$.

$u_o(x) = \sin \pi x$; prescribed ata at $x = -1$, outflow at $x = 1$.

CFL = 0.8 , t = 2.

r_c is the "numerical order of accuracy."

	J	r = 2	r_c	r = 3	r_c	r = 4	r_c	r = 5	r_c	r = 6	r_c
L_∞ - Error	8	1.602×10^{-1}		3.990×10^{-2}		1.846×10^{-2}		6.652×10^{-3}		8.481×10^{-3}	
			1.08		3.12		2.91		5.04		6.28
	16	7.581×10^{-2}		4.593×10^{-3}		2.447×10^{-3}		2.018×10^{-4}		1.091×10^{-4}	
			1.12		2.85		2.91		4.98		5.20
	32	3.488×10^{-2}		6.374×10^{-4}		3.251×10^{-4}		6.386×10^{-6}		2.972×10^{-6}	
			1.20		2.93		3.08		4.78		5.11
	64	1.519×10^{-2}		8.35×10^{-5}		3.845×10^{-5}		2.312×10^{-7}		8.620×10^{-8}	
L_1 - Error	8	1.374×10^{-1}		3.378×10^{-2}		1.335×10^{-2}		8.691×10^{-3}		6.632×10^{-3}	
			1.68		3.19		3.43		5.29		6.34
	16	4.299×10^{-2}		3.697×10^{-3}		1.234×10^{-3}		2.227×10^{-4}		8.209×10^{-5}	
			1.67		2.84		3.66		5.13		6.39
	32	1.354×10^{-2}		5.166×10^{-4}		9.742×10^{-5}		6.373×10^{-6}		9.807×10^{-7}	
			1.76		2.88		3.76		5.18		6.01
	64	3.995×10^{-3}		6.994×10^{-5}		7.201×10^{-6}		1.763×10^{-7}		1.524×10^{-8}	

Table 2. Mesh Refinement for 4-th Order ENO with Exponential Data.

$u_t + u_x = 0$, $u(x,0) = e^{-x}$; $u(-1,t) = e^{1+t}$; outflow BC at x=1.

CFL = 0.4 , t = 1.

J	20	40	80	160	320	640
L_∞ -error	5.063×10^{-4}	3.968×10^{-4}	4.148×10^{-4}	1.986×10^{-5}	2.648×10^{-6}	5.060×10^{-7}
L_1-error	2.905×10^{-4}	1.664×10^{-4}	9.132×10^{-5}	9.257×10^{-6}	9.648×10^{-7}	1.737×10^{-8}

Standard Bibliographic Page

1. Report No. NASA CR-178206 ICASE Report No. 86-69	2. Government Accession No.	3. Recipient's Catalog No.
4. Title and Subtitle ON THE NONLINEARITY OF MODERN SHOCK-CAPTURING SCHEMES		5. Report Date October 1986
		6. Performing Organization Code
7. Author(s) J. H. Morrison, M. Napolitano		8. Performing Organization Report No. 86-69
9. Performing Organization Name and Address Institute for Computer Applications in Science and Engineering Mail Stop 132C, NASA Langley Research Center Hampton, VA 23665-5225		10. Work Unit No.
		11. Contract or Grant No. NAS1-17070, NAS1-18107
12. Sponsoring Agency Name and Address National Aeronautics and Space Administration Washington, D.C. 20546		13. Type of Report and Period Covered Contractor Report
		14. Sponsoring Agency Code 505-90-21-01

15. Supplementary Notes

Langley Technical Monitor:
J. C. South

Submitted to Proc. of Wave Motion: Modeling, theory, and computations

Final Report

16. Abstract

In this paper, we review the development of shock-capturing methods, paying special attention to the increasing nonlinearity in the design of numerical schemes. We study the nature of this nonlinearity and examine its relation to upwind differencing. This nonlinearity of the modern shock-capturing methods is essential, in the sense that linear analysis is not justified and may lead to wrong conclusions. Examples to demonstrate this point are given.

17. Key Words (Suggested by Authors(s))	18. Distribution Statement
conservation laws, shock-capturing, essentialy non-oscillatory	02 - Aerodynamics 59 - Mathematic and Computer Science (General) Unclassified - unlimited

19. Security Classif.(of this report)	20. Security Classif.(of this page)	21. No. of Pages	22. Price
Unclassified	Unclassified	62	A04

For sale by the National Technical Information Service, Springfield, Virginia 22161

NASA-Langley, 1986